ADVANCED FUNCTIONAL MATERIALS
www.afm-journal.de

Toward Scalable Solutions for Silver-Based Gas Diffusion Electrode Fabrication for the Electrochemical Conversion of CO_2 – A Perspective

Simon Emken, K. Ashoke Raman, Alexander Bauer, Violeta Karyofylli, Eva Jodat, André Karl, and Rüdiger-A. Eichel*

The electrochemical reduction of carbon dioxide (eCO_2R) has attracted considerable research interest in recent years due to its potential application in decarbonizing industry and transportation. Silver-based gas diffusion electrodes (GDEs) are one of the most promising cathode variants for electrolysis at industrially relevant current densities, producing carbon monoxide (CO) with high Faradaic efficiencies (FE). A major challenge on the way to commercialization of the technology is the scale-up of the cathode designs. In this study, a systematic literature review of the published work on eCO_2R in the past decade (2015–2025) is performed to identify the main techniques for the fabrication of silver-based GDEs and the design and performance of the corresponding electrodes are summarized. The fabrication methods in terms of scalability is compared and an overview of recent scaling efforts is provided. Based on the findings, a perspective is provided on the main challenges of scaling eCO_2R and viable solutions are discussed. In addition, recent advances in physics-based and data-driven modeling of eCO_2R are reviewed and discussed to give a perspective on how modeling coupled with experimental work benefits the accelerated development and paves the way for industrial deployment of CO_2 electrolyzers.

1. Introduction

The need for energy storage, energy carriers, fuels, and basic chemicals with a focus on utilizing renewably generated electricity increases steadily due to the growing demands of Earth's society and the highly detrimental consequences of climate change caused by excessive anthropogenic carbon emissions. To mitigate the continued increase of the carbon dioxide concentration in the atmosphere, it is crucial to steer away from both fossil-based energy sources and chemical feedstocks as much as possible, and to reduce emissions by capturing carbon dioxide (CO_2) from point sources and directly from ambient air.[1,2] The electrochemical conversion of CO_2 is considered to be a key technology for the utilization of renewably generated electricity to produce valuable chemicals, such as formic acid, ethylene, or carbon monoxide (CO), for example, while significantly decreasing net CO_2 emissions. The development of catalysts, electrodes, and cell designs for this technology has gained steadily increasing attention and relevance in the research community since 2010.[3] The cathode is the key component in electrochemical CO_2 conversion cells, and the best-performing variant is the gas diffusion electrode (GDE), which was derived from polymer electrolyte fuel cell technology development.[4–6]

With respect to the future economic feasibility of electrochemical CO_2 conversion, the key metrics to target are a low cell voltage, comparable to proton exchange membrane (PEM) electrolysis (<2 V), and reasonable stability (>5 years)[7] at current densities that exceed 200 mA cm^{-2}.[8] In a valorization study in which CO was compared to formic acid or ethylene by Detz et al., it was estimated that by 2030, electrolytically produced CO might be cost-competitive for specialty chemicals in comparison to fossil-derived CO, for example.[9] For detailed studies on economic analyses, which are beyond the scope of this article, we refer the readers to published works.[10,11] Further, with respect to research topics beyond the scope of silver-based GDE development, we recommend considering some of the detailed review articles.[12–14]

S. Emken, K. A. Raman, A. Bauer, V. Karyofylli, E. Jodat, A. Karl, R.-A. Eichel
Institute of Energy Technologies
Fundamental Electrochemistry (IET-1)
Forschungszentrum Jülich
52425 Jülich, Germany
E-mail: a.bauer@fz-juelich.de
S. Emken, R.-A. Eichel
Institute of Physical Chemistry
RWTH Aachen University
52062 Aachen, Germany
R.-A. Eichel
Faculty of Mechanical Engineering
RWTH Aachen University
52062 Aachen, Germany

The ORCID identification number(s) for the author(s) of this article can be found under https://doi.org/10.1002/adfm.202522386

DOI: 10.1002/adfm.202522386

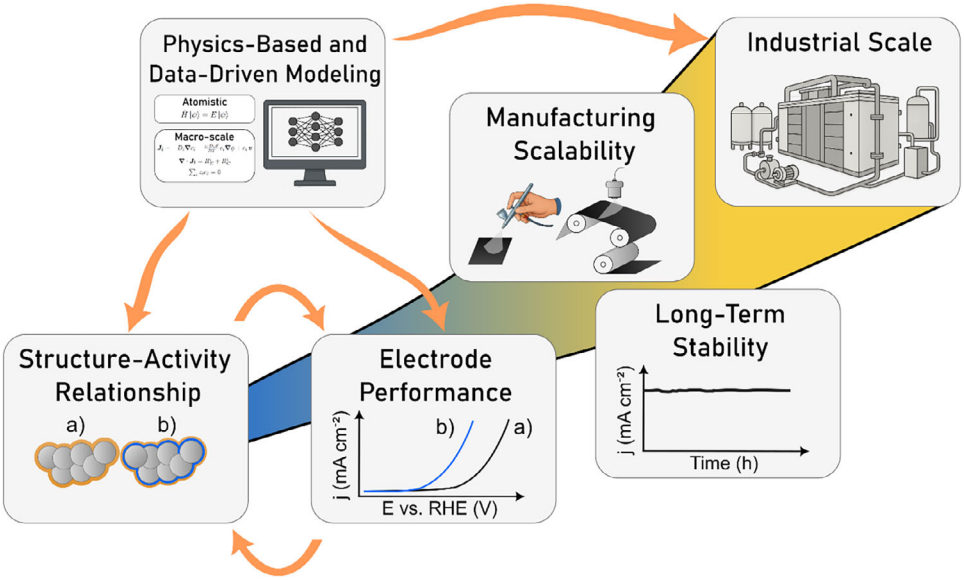

Figure 1. Overview of how physics-based and data-driven modeling can help pave the way for the commercialization of low-temperature CO_2 electrolysis.

In this perspective, we discuss the state of the art with respect to the preparation of silver-based GDEs, specifically applied for the production of CO, as well as the structure-activity relationships governing their performance. We conducted a systematic literature survey, focusing on the past decade of experimental work. This information is complemented by an overview of the most relevant works in the modeling and artificial intelligence domains. We identify ink-based methods as the most commonly applied manufacturing techniques for silver-based GDEs and found a significant catalyst loss in published works. The catalyst loss not only leads to waste, which is discussed in the framework of a potentially circular economy, but also to a mismatch between the ink and catalyst layer composition. Further, we offer our perspective on the preferred electrode and cell design, as well as scaling efforts, in particular regarding which techniques are best suited for electrode fabrication in continuous mode with industrially relevant electrode dimensions. In our opinion, the development of hybrid physics-based and artificial intelligence (AI) models can greatly improve the development of CO_2 electrolyzers toward commercialization.

Figure 1 shows the conceptual framework of this perspective: As illustrated, understanding structure-activity relationships can lead to enhanced electrode performance (Section 2.5). Moreover, long-term stability and appropriate manufacturing techniques are necessary for deployment on an industrial scale (Sections 3 and 4). Finally, physics-based and data-driven modeling can assist optimization, prediction, and deduction processes in all stages (Section 5).

2. Overview and State of the Art Regarding Experimental Work on Silver-Based Gas Diffusion Electrodes

The electroreduction of carbon dioxide to carbon monoxide is a diverse area of research, which is also reflected in the variety of electrode designs used in electrolysis experiments. Based on a systematic literature review, an overview of the current directions in the fabrication of silver-based electrodes for CO_2-to-CO electrolysis is given in this section.

2.1. Literature Analysis

A literature review of published work from the past 10 years (2015–2025) was conducted to evaluate the electrode designs and fabrication methods used in silver-based electroreduction of carbon dioxide. The methodology was similar to previously reported studies.[15,16] Accordingly, 477 publications were sourced by specifying a topic ("Electrochemical reduction of CO_2" and variations/synonyms) and defining search terms with respect to the abstracts ("Ag electrocatalyst" or "gas diffusion electrode" and variations/synonyms) in Web of Science, as schematically shown in **Figure 2**. Details of the Web of Science search, including a link, are given in the Supporting Information. The keywords "gas diffusion electrode" were added to include publications in which the electrocatalyst was not specified in the abstract. Consequently, studies in which silver-based catalysts were not used were excluded, resulting in 154 publications. To supplement the dataset, additional publications were included by adding cited references from the 154 publications that were reported in the main text of the respective publications in tabular or graphical form for comparison. These references were only included if a silver-based electrocatalyst was used in the respective study and the maximum reported partial current density for the formation of carbon monoxide j(CO) exceeded 50 mA cm^{-2}. Following this procedure, a dataset of 166 publications was obtained. In the dataset, silver-based tandem electrodes (Ag + other metal) were used in three studies,[17–19] in one study, a silver-based electrocatalyst for the conversion of CO_2 to multi-carbon products was investigated,[20] and in another study, indirect electroreduction via bromoethanol was reported.[21] From these publications, only metadata on the

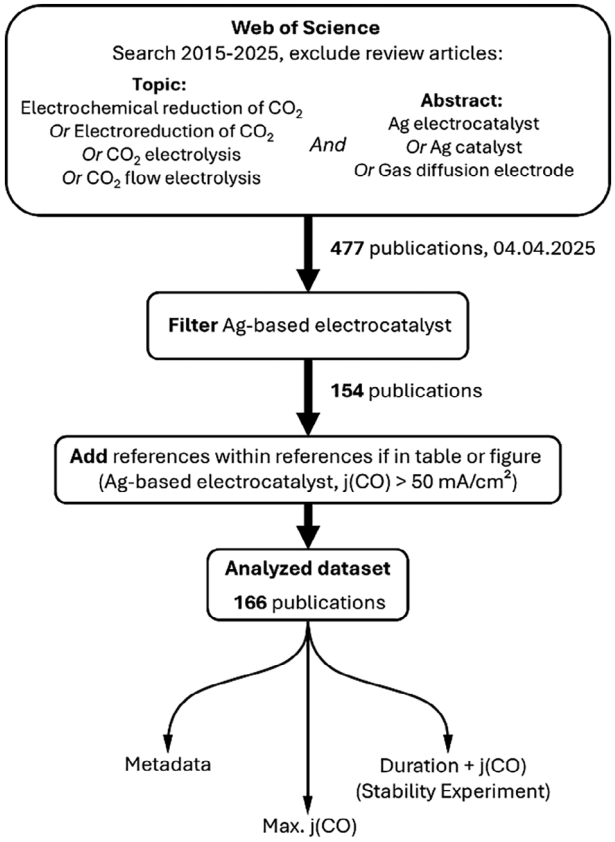

Figure 2. Overview of the literature search workflow. 477 publications were retrieved using Web of Science by filtering based on publication year (2015–2025), topic, and abstract. Publications that did not feature Ag-based electrocatalysts were excluded. In addition, cross-references that were cited in the publications in tables or figures were included in the dataset if Ag-based electrocatalysts were used and the partial current density for CO exceeded 50 mA cm^{-2}.

experimental setup and the preparation method were extracted, but not performance data. From the other studies with a focus on CO_2-to-CO electrolysis, both metadata on the fabrication method and cell operation and performance data, such as the duration of long-term electrolysis experiments and the maximum reported partial current density for CO generation (max. j(CO)), were extracted. The dataset, including extracted metadata and specific data, is provided in the Supporting Information.

Figure 3a shows that most stability studies were conducted for less than 24 h, with only 8 stability experiments lasting longer than one week (168 h).

Figure 3b illustrates the electrode support materials used, which have been grouped into five categories: Carbon-based gas diffusion layers (GDLs) are by far the most widely used in CO_2 electrolysis, although problems with stability (electrowetting, flooding, and salt precipitation) were frequently reported.[22–27] The second most widely used electrode supports are metal foils and plates (mainly Ag foils), which were used exclusively in H-type cell experiments at lower current densities, since the electroreduction is limited by the solubility and diffusion of CO_2 in aqueous media.[28,29] They were included in the dataset to provide a broader overview of Ag-based electroreduction of CO_2. Porous metals, meshes, or woven fabrics (all metal-based) were investigated as electrode substrates in 18 publications. Examples include Ag hollow fibers,[30] Ag particles with PTFE deposited on a Ni mesh,[31] and commercial silver filtration membranes.[32] In addition, GDEs based on fluorinated polymer membranes (especially PTFE) are widely used, originally motivated by the potential to overcome stability problems encountered with carbon-based GDEs.[33,34] The remaining publications either could not be assigned to any of the four introduced electrode substrate categories, or there was no reported information on the electrode structure and the substrate (12 publications). For instance, in refs.[35–37] glassy carbon (carbon-based, but without a GDL) was applied, and in ref. [38], a commercial electrode from Gaskatel was used.

Figure 3c shows the reported cell size expressed by the geometric electrode area in contact with the electrolyte. Only in three studies was information on electrolyzers with a geometric active electrode area greater than 50 cm^2 reported, while in 113 publications, the electrode area was below 10 cm^2 (predominantly 1 cm^2, see literature dataset). The three studies with an electrode area larger than 50 cm^2 include two papers by Endrődi et al.[39,40] in which 61 cm^2 (stack) and 100 cm^2 cells were investigated, and the study by Krause et al., in which a 300 cm^2 cell developed by Siemens Energy was operated.[41]

Figure 3d shows the catholyte/electrolyte used in three-electrode setups, H-type cells, and GDE setups (in zero-gap and membrane electrode assembly (MEA) configurations, only gas is supplied to the cathode). Accordingly, $KHCO_3$ was most frequently used in the dataset, indicating that most investigations were conducted at near-neutral bulk pH. In the second group of studies (25 publications), alkaline KOH was used as the catholyte, with the advantage of suppressing detrimental hydrogen evolution and reducing the cell voltage, but inevitably favoring the carbonation of CO_2, as shown in Equation (1).

$$2\ OH^-_{(aq)} + CO_{2\,(g)} \rightarrow CO^{2-}_{3\,(aq)} + H_2O_{(l)} \quad (1)$$

Accordingly, alkaline catholyte cells do not operate under steady state conditions, because there is a continuous consumption of hydroxide ions. In addition, carbonate formation also occurs in neutral bulk pH catholyte due to the generation of hydroxide ions according to Equation (2).[12,42,43]

$$\mathbf{CO_{2(aq)} + H_2O_{(l)} + 2e^- \rightarrow CO_{(aq)} + 2OH^-_{(aq)}} \quad (2)$$

Depending on the cell architecture, these carbonate ions are protonated to release CO_2 again in different parts of the cell. In anion exchange membrane (AEM) cells, the carbonate ions cross the membrane to react with the protons generated at the anode, limiting the carbon conversion efficiency in these CO_2-to-CO electrolyzers to a maximum of 50%. Two hydroxide ions are formed at the cathode per reduced CO_2 molecule, as shown in Equation (2), which in turn form one carbonate ion as presented in Equation (1).[32,42,44] Finally, it is noteworthy that in some studies, different salts were used, including a mixture of sulfuric acid and potassium sulfate for the acidic electrolysis of CO_2.[45,46]

The cell types employed in the literature dataset are reported in Figure 3e and have been classified according to the scheme proposed by Alinejad et al., shown in **Figure** 4, with the exception

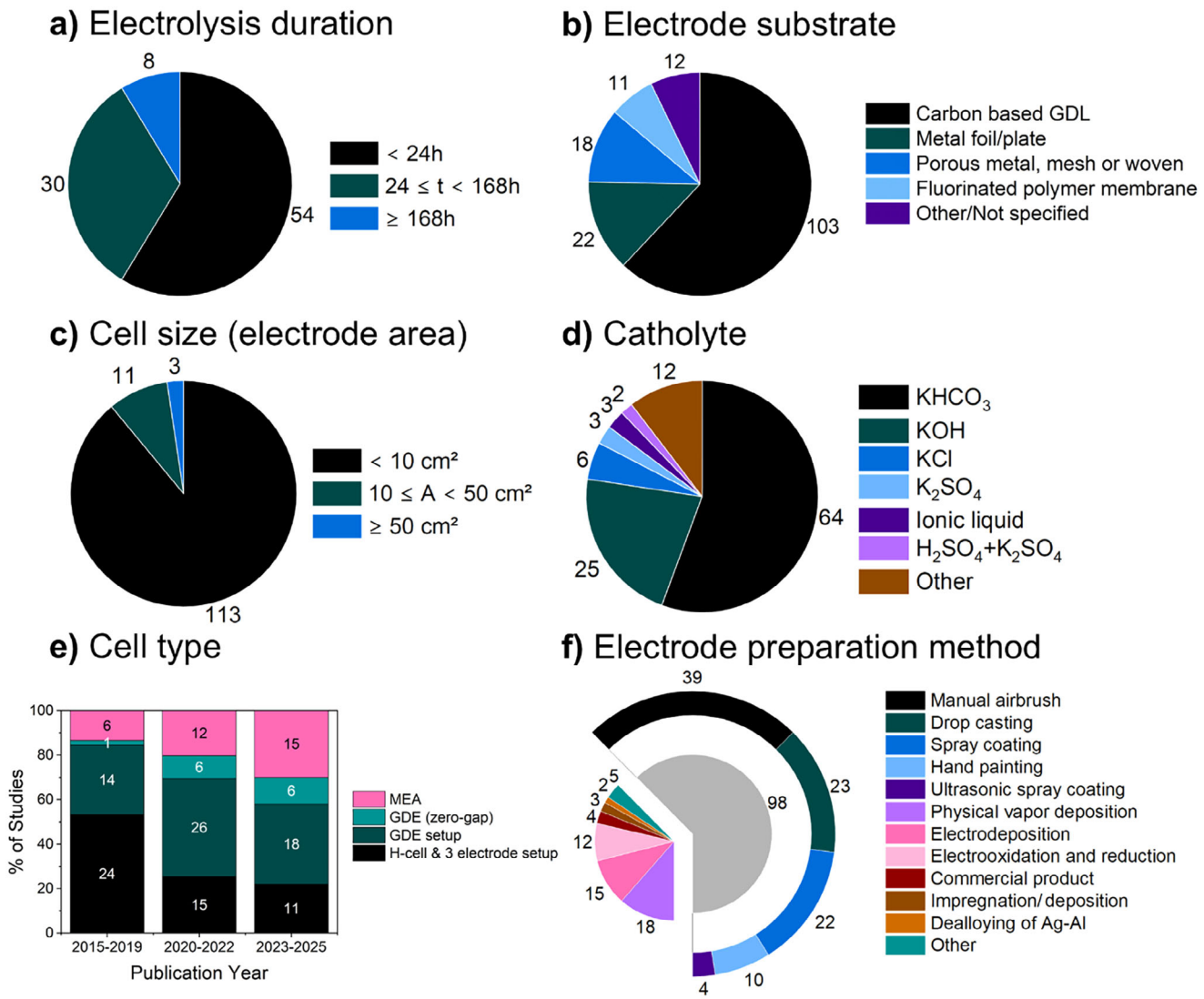

Figure 3. Analysis of literature-based dataset on CO_2 electrolysis, including exclusively studies in which Ag-based electrocatalysts were used. Data labels indicate the absolute number of publications. Note that the sum of the data labels does not always equal the number of publications in the dataset (166), as not every aspect investigated was reported in each study. a) Reported electrolysis time in long-term experiments. b) Substrate used for electrode fabrication. c) Cell size/geometric electrode area used. d) Catholyte used for non-MEA and non-zero-gap configurations. e) Cell type as a function of publication year. f) Method of electrode preparation.

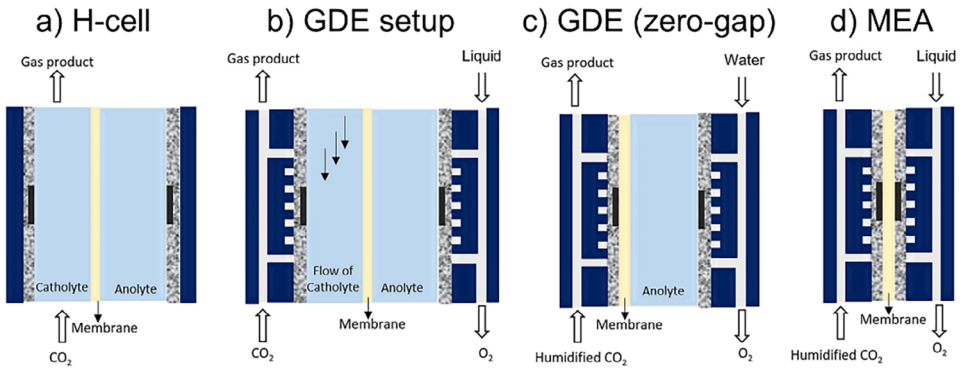

Figure 4. Classification of cell configurations for the electroreduction of CO_2 proposed by Alinejad et al. Reproduced under terms of the CC-BY license.[47] Copyright 2024, The Authors, published by Elsevier.

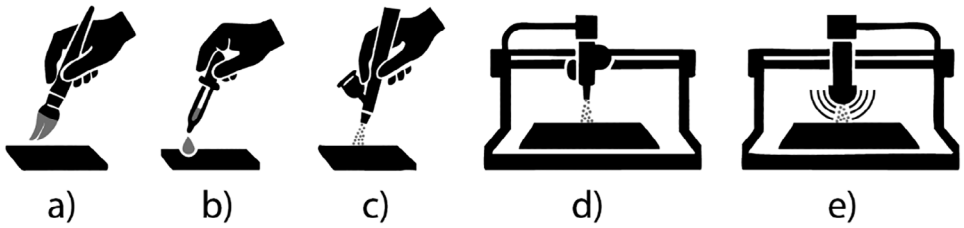

Figure 5. Schematic of ink-based electrode fabrication methods: a) manual hand painting, b) drop casting, c) manual airbrushing, d) automated spray coating, and e) ultrasonic spray coating.

that rudimentary three-electrode setups were included in the H-cell category.[47] In H-cells (Figure 4a), CO_2 must diffuse through a liquid electrolyte to the cathode, while in the other three configurations, gaseous CO_2 is supplied to GDEs. In the typical GDE configuration (Figure 4b), the anode and cathode compartments of the cell are separated by a membrane, which also separates the catholyte and anolyte streams.

To reduce the concentration overpotential of the cathode, the liquid catholyte can be replaced by a humidified CO_2 supply, which is the key feature of zero-gap designs (Figure 4c). The cathode is then attached directly to the membrane.[48–50] This idea is further developed in MEA cells, where both the anode and cathode are in direct contact with the membrane (Figure 4d).[51–54] It should be noted that the classification scheme does not include configurations where only the anode is configured as a zero-gap design, as in ref. [55]. In addition, in some studies, microfluidic cells were used without a membrane and only one electrolyte that contacts both anode and cathode.[56,57] For this analysis, both configurations were associated with the conventional GDE setup (Figure 4b).

From Figure 3e, it can be inferred that the use of zero-gap and MEA designs has increased over the past 10 years and that H-cell experiments are becoming less common. Furthermore, several flow-through electrodes were used in configurations that are identical or close to H-cell designs and have therefore been attributed to H-cell setups, despite their characteristic direct supply of gaseous CO_2 to the cathode.[30,58–60]

Figure 3f shows the analysis of the electrode preparation methods. When multiple methods were employed to fabricate the electrode in a single study, each of them was counted. Physical vapor deposition (PVD) methods (sputtering, electron beam evaporation, and thermal evaporation) were used in 18 studies to deposit thin films of catalyst materials onto GDLs.[33,61–63] In addition, electrodeposition and impregnation/deposition techniques were applied in several studies.[64–68] Electrooxidation and reduction treatments were almost exclusively used to implement microstructured surfaces of Ag foils and plates.[69–71] Notably, in two publications, the fabrication of porous silver substrates by dealloying of Ag—Al was reported.[72,73] Furthermore, commercial GDEs were used as cathodes in four publications.[38,53,74,75]

Clearly, ink-based methods (highlighted in the ring in Figure 3f) are at the forefront for the preparation of silver-based electrodes in CO_2 electrolysis. These methods include a) manual hand painting, b) drop casting, c) manual airbrushing, d) spray coating, and e) ultrasonic spray coating, which are visualized in **Figure 5**.

Studies in which spray coating was reported as the preparation method often lacked equipment specifications, leading to uncertainty as to whether ultrasonic spray coating, an automated spray coating process, or manual airbrushing was used. Therefore, it is highly recommended to include a description of the spray coating device in the experimental section. In this study, spray coating is defined as an automated spray process, e.g., the automated airbrush setup used in studies[56,76–81] is also associated with this method. It should also be noted that the spin coating process used in refs. [35,36] is attributed to the "drop casting" method, because, according to the description given, the ink was applied drop by drop, and equipment specifications were not mentioned. From Figure 3f, it can be concluded that manual airbrushing was most frequently used for the fabrication of Ag-based GDEs for the electroreduction of CO_2, followed by drop casting, spray coating, and hand painting. Ultrasonic spray coating processes were used in four studies only.

2.2. Catalyst Loss with Ink-based Methods: Mismatch Between Ink and Catalyst Layer Composition

When ink-based methods are applied, the catalyst is usually dispersed, and a (pre-dissolved) binder polymer is added before the mixture is ultrasonicated to homogeneously disperse the nanoparticulate material. This ink is then deposited onto the electrode substrate/GDL to obtain the catalyst layer.[24,52,56,82–85]

Figure 6 shows the extent to which the composition of the catalyst layer was characterized in the studies in which ink-based methods were used. Note that there is a discrepancy between the total number of studies in Figure 6 (95) and the number of studies in which ink-based methods are used (Figure 3f, 98) because

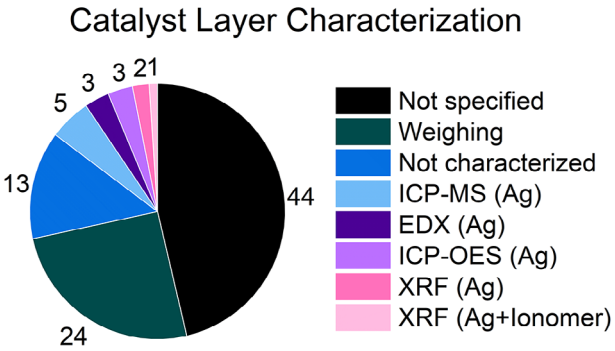

Figure 6. Overview of the catalyst layer characterization techniques used in the analyzed literature dataset.

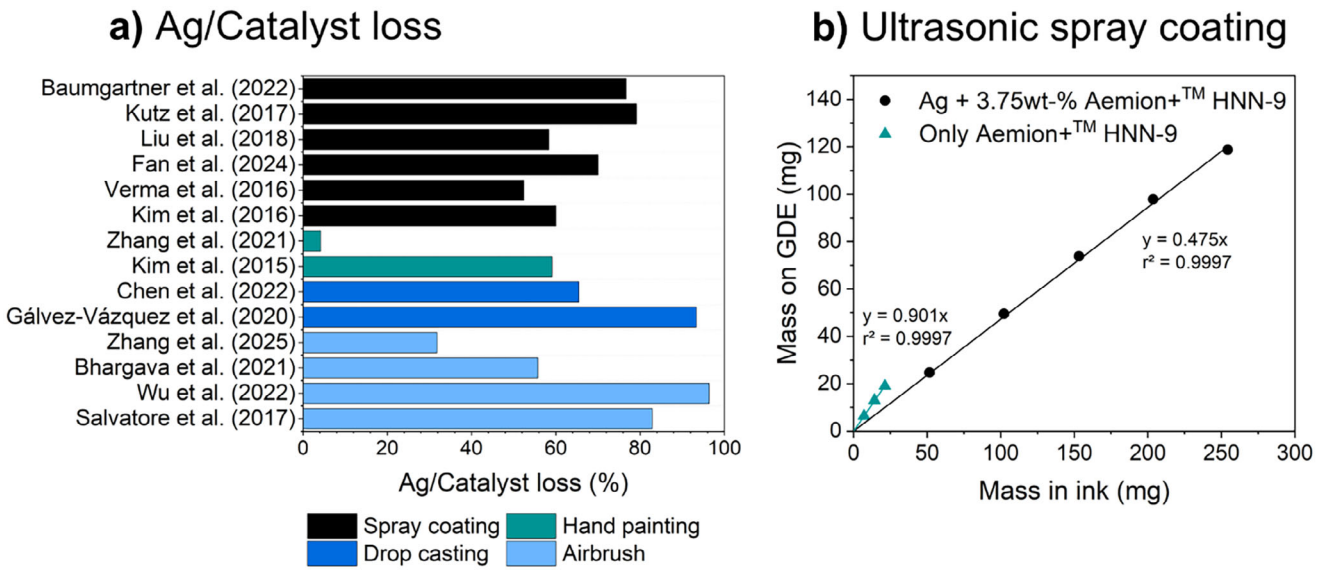

Figure 7. a) Ag nanoparticle/catalyst loss during electrode preparation by hand painting, drop casting, spray coating, and airbrushing. Catalyst loss was calculated from information given in the experimental sections of the respective publications using Equation (3).[6,56,57,76,79,80,93–100] b) Relationship between mass in ink and mass deposited on GDE by ultrasonic spray coating (Nadetech ND-SP equipped with ultrasonic nozzle) using Ag nanoparticles + 3.75 wt-% Aemion+ and only the ionomer in the ink. Ethanol/acetone 65:35 (wt/wt) was used as an ink solvent. For experimental details, see the Supporting Information.

in two studies, multiple ink-based methods were used.[83,86] It is common practice to report the mass loading by weighing the electrode before and after the deposition process. However, in some references, such information was not reported ("not characterized"). Only in one study was information on the composition of the catalyst layer reported, by determining both the Ag loading and the Nafion loading by X-ray fluorescence spectroscopy (XRF). To our knowledge, there are no studies in which both the mass loading (loading of Ag catalyst and ionomer) and elemental analysis results regarding the Ag content (e.g., by inductively coupled plasma optical emission spectroscopy (ICP-OES) or mass spectrometry (ICP-MS) or energy-dispersive X-ray spectroscopy (EDX)) were reported, which in principle would also allow two-component analysis. In most studies, the loading was reported, but not the characterization method ("not specified"). Since no apparatus was specified in these cases, likely, the electrodes were simply weighed before and after the deposition process.

There can be significant variations in the composition of the ink compared to the corresponding catalyst layers. For example, Bühler et al. prepared IrO_2+Nafion inks and sprayed them onto a substrate by ultrasonic spray coating. After deposition, they performed thermogravimetric analyses of the GDEs to determine the Nafion content. Counterintuitively, the measured Nafion content was approximately five times higher than expected.[87] It was hypothesized that the significant deviation was caused by the precipitation of the dispersed catalyst nanoparticles in the syringe and spray coater tubing during the spraying process, which is supported by Mayerhöfer et al.[88,89] The described catalyst loss can be considered as inherent to ink-based methods, as indicated by **Figure** 7a. It shows the loss of catalyst material, which was calculated in this study based on the reported experimental details of a selection of publications from the literature dataset. In these studies, a detailed description of the experimental procedures was given, including the area of the sprayed-on substrate A, the complete ink formulation (solid content $m_{Ag/solid}$), and the measured loading (Γ, weighing of the electrode before and after deposition or Ag analysis). The catalyst loss x (including additives, such as the ionomer and particulate carbon) is then calculated using Equation (3).

$$x = m_{Ag/solid} - \Gamma \cdot A \quad (3)$$

when the electrode was weighed before and after deposition, $m_{Ag/solid}$ refers to the total mass of solid in the ink, while in the case of elemental analysis, only the mass of Ag particles in the ink is considered. Details of the experimental procedures, ink formulations, and the calculated losses are given in the literature dataset. Significant losses of catalyst material occur with all four methods, ranging from 5% to over 90%. For the spray methods, in addition to catalyst nanoparticle precipitation, a part of the loss may also be due to spraying over the edges of the substrate, especially in the case of manual airbrushing. In view of these significant losses, and in the context of the hypothesis invoked by Bühler et al. and Mayerhöfer et al., the composition of the catalyst layer likely differs from the ink composition in many studies. The extent of the deviation between the ink and catalyst layer composition likely varies depending on the experimental setup, e.g., the spraying method used, the ultrasonication procedure, the spraying time, etc. This deviation seems to be related to agglomeration and/or sedimentation of the Ag nanoparticles and the ionomer.

Baumgartner et al. mitigated the expected precipitation of Ag nanoparticles in the ink by roughly tripling the amount of required nanoparticles (desired loading of 1 mg cm^{-2} for 3 × 3 cm^2, but 33 mg nanoparticles in the ink). A Nafion content of 20 wt% in the catalyst layer was desired, so 180 µl of a 5 wt% solution (≈9 mg Nafion) was incorporated into the ink. Following the

suggestion by Bühler et al. and Mayerhöfer et al. that mainly Ag nanoparticles precipitate, while the binder remains dissolved/dispersed, it is likely that the actual Nafion content in the catalyst layer is significantly higher than in the ink.[79,81,90] Interestingly, even the use of an ultrasonic syringe, which is designed to maintain dispersion during the spraying process, resulted in a significant deviation between the ink and the catalyst layer composition.[86]

To further explore the effect on the catalyst layer composition, silver GDEs were prepared in this study by ultrasonic spray coating using a formulation containing silver nanoparticles, Aemion+ HNN-9 ionomer, and ethanol/acetone, similar to a formulation reported in the literature.[55] Figure 7b shows that when only the ionomer (Aemion+ HNN-9 is soluble in ethanol/acetone) was in the ink, ≈90% of it was deposited on the electrode. However, in the catalyst ink containing silver nanoparticles and 3.75 wt% of the same ionomer (based on catalyst mass), only 47% of the mass (Ag nanoparticles + ionomer) was deposited onto the electrode. Due to the high mass fraction of Ag nanoparticles in the ink, a first approximation shows that half of the silver nanoparticles were not deposited onto the electrode. Based on our observations, the hypothesis by Bühler et al. and Mayerhöfer et al. that nanoparticle precipitation is the main cause of the high losses is supported. In the Supporting Information, a photograph (Figure S2, Supporting Information) is included, which shows the precipitated nanoparticles remaining in the syringe after the spraying process. Assuming that ≈90% of the ionomer and ≈50% of the silver nanoparticles were deposited onto the electrode in our system, a 3.75 wt% ionomer content in the ink resulted in almost double the content (6.3 wt%) in the catalyst layer. In our opinion, this difference in composition is not negligible, especially in light of recent studies emphasizing the role of the ionomer with respect to the mass transport through and the stability of GDEs.[54,86,91,92]

Besides using an ultrasonic syringe, the catalyst loss may also be reduced by stabilizing the catalyst ink with polymeric agents, e.g., functionalized methylcellulose on an industrial level[31,101–104] or by applying the ink via vacuum filtration in lab-scale experiments,[105,106] which can result in reduced losses ≈25%.[107] In addition, it was shown that for inks containing iridium oxide nanoparticles that ball milling with zirconium oxide beads can significantly increase the corresponding ink stability.[108] In our opinion, the development of Ag-based metal organic decomposition (MOD) inks also seems intriguing, as no particulate matter is dispersed, but a dissolved precursor Ag-complex is sprayed on the substrate, which is subsequently reduced at moderate temperatures (<150 °C).[109] In that case, it will most likely be necessary to introduce sufficient porosity in the catalyst layer.

2.2.1. Resource Demands and Recycling Strategies

Although silver is less expensive compared to other transition metals like platinum and iridium, it is reasonable to assume that the catalyst loss in the fabrication procedure of the cathode will have a significant impact on the cost of the whole electrolyzer unit. To give an estimation of Ag-usage per electrolyzer power input, the performance data of the study by Shin et al. is considered (cell voltage 2.6 V, 500 mA cm^{-2}, Ag loading 2.0 mg cm^{-2}), which is comparable to other recent techno-economic assessments.[110–112] Depending on the catalyst loss, the Ag usage would vary between 1.5 (no catalyst loss) and 4.1 kg MW^{-1} (63% catalyst loss, average from Figure 7a). Besides the higher cost, the consequence on an industrial level would be the implementation of process steps to retrieve the catalyst lost in the fabrication. As these particles have agglomerated, recycling would necessitate de-agglomeration and redispersion, e.g., by bead milling and/or ultrasonication.[113,114] Therefore, not complicating the recycling process should also be considered a design factor for catalyst inks.

It is worthwhile to discuss the material consumption for cathode manufacturing also in the broader context of low-temperature CO_2 electroreduction. As given in **Table 1**, we compared the resource availability and cost of the commonly applied catalyst materials silver (carbon monoxide), copper (ethylene, multicarbon products),[34,115–117] tin, and bismuth (formic acid).[117–119] As Ag, Cu, and Sn are metals used commercially in large volumes, their end-of-life recycling rate is higher compared to Bi. To put these data into perspective, we conducted a simplified calculation of the metal demand for cathode manufacturing, based on the market size of the CO_2 electroreduction products and the electrolyzer models by Shin et al. (metal loading 2 mg cm^{-2}).[110] In this scenario, the installation of CO_2 electrolyzers to fulfill current market requirements for CO, formic acid, and ethylene would require 75.8 t Ag, 1240 t Cu, and 1.62 t of Sn or Bi, respectively. These demands represent shares of the respective current annual mining production in the range from several ppm to well below 1%. Overall, the brief discussion suggests that metal resource limitations for the cathode are not likely to be expected. Instead, the iridium potentially used for the anode has to be seen as the limiting factor, which is indeed discussed in the PEM water electrolysis literature.[120] On the other hand, using abundant Ni as an anode catalyst would circumvent these limitations (see Table S3, Supporting Information).

Still, non-silver alternatives for the electrochemical conversion of CO_2 to CO should be considered as a viable option to reduce raw material use and cost, especially considering future market developments. In fact, the Silver Institute reported a yearly silver deficit of ≈3000–7000 t since 2021.[128] Moreover, besides its use for jewelry and the photographic industry, silver is an important raw material in the strongly growing electronics and photovoltaics sector.[129] It was estimated that the installation of 15–60 TW photovoltaic capacity by 2050 could amount to using 85–98% of current global silver reserves. In another study, it was highlighted that an annual increase of the silver end-of-life recycling rate by 1% could eliminate the supply shortage.[130,131] Research with respect to silver alternatives has focused on two directions: metal-free defective carbon catalysts doped with heteroatoms,[132,133] and single-atom catalysts based primarily on first row transition metals like iron, nickel, and cobalt.[134–136] Recently, dual and multi-atom catalysts have also been studied for electrocatalytic applications, including eCO_2R.[137–140] These silver-free alternatives start to achieve industrially relevant current densities. For example, a nitrogen-, sulfur-, phosphor-doped porous carbon catalyst was tested successfully in a flow cell for 14 h (180 mA cm^{-2}, >90% FE(CO))[141]

Table 1. Resource availability and recycling data of promising catalyst materials for low-temperature CO_2 electrolysis in the context of the market volume of the corresponding CO_2 electroreduction product.

Parameter	Ag	Cu	Sn	Bi
CO_2 electroreduction product	Carbon monoxide	Ethylene (C_{2+})	Formic acid	Formic acid
Abundance in Earth's crust (10^{-4} wt-%)[121]	0.07	47	2.5	0.009
World mining production (t)[122]	25000	23000000	300000	16000
Reserves (t)[122]	640000	980000000	>4200000	–
Old scrap collection rate (%)[123]	76, 77, >80 [a)]	24, 78	50	<1[a)]
Recycled content (%)[123]	20, 30, 32	20, 30, 37	22	–
End-of-life recycling rate (%)[123]	58, 97, 30–50 [a)]	43, 53	75	<1[a)]
Price (US$ t^{-1})[124]	1504000	10233	34749	–
Catalyst demand per ton of annual production capacity based on models by Shin et al.[110] (g t^{-1})	0.959	3.90	1.63	1.63[b)]
Market size of product (10^6 t)	≈79[c)] (2022)	316.8 (2023)[125]	0.995 (2024)[126]	0.995 (2024)[126]
Catalyst demand (t) (Share of world mining production, ppm)	75.8 (3031)	1240 (54)	1.62 (5.4)	1.62 (101)

[a)] Estimated by the United Nations Environment Programme expert group; [b)] The model by Shin et al. for formic acid included only Sn; we assume equal performance data for a Bi-based electrocatalyst; [c)] CO market size is estimated based on stoichiometry and the methanol market size of 90 Mio t in 2022.[127]

and a nickel-based single atom catalyst was tested for 120 h (300 mA cm^{-2}, 90% FE(CO)).[142,143] The upscaling of the catalyst synthesis methods will be a significant challenge.[140,144]

In the framework of a potentially circular economy, recovering raw materials from the used GDEs is critical. To the best of the authors' knowledge, recycling strategies for silver-based GDEs have not yet been investigated in the scientific literature. The process design will depend heavily on the electrode structure and composition. Nonetheless, it is likely that recycling strategies for PEM water electrolysis MEAs can also be largely adopted for silver-based GDEs and MEAs. Recently, a complete recycling chain was reported for PEM water electrolyzer stacks, including a leaching step with aqua regia.[145] These leaching processes may have a negative environmental impact (e.g., leaching with aqua regia produces highly toxic and corrosive gases). As an alternative, Carmo et al. developed a recycling reactor in which the catalyst layers were delaminated by an ultrasonic treatment in two separate chambers while simultaneously preserving the membrane. The membrane and the recycled catalyst particles were also retested, with only slight performance losses observed in the polarization curve.[146] Such a process would be desirable also for silver-based GDEs/MEAs. If performance losses become significant after recycling, a more sustainable leaching process could utilize fatty acids, as recently demonstrated.[147]

2.3. Electrode Structures for CO_2 Electrolysis and their Modification

Based on the definition of the electrode substrate classes in Figure 3b, four categories of electrode structures used in low-temperature CO_2 electrolysis can be defined as shown in **Figure 8**. The first type is based on metal foils and plates and can only be used in H-type cells due to the lack of a GDL (Figure 8a,b). This group of electrodes is typically prepared either by performing electrochemical oxidation and reduction steps on Ag foils and plates to obtain activated nanostructures on the surface[69,70,148,149] or by electrodepositing Ag particles from solution onto the electrode.[67,68,150]

The second category represents a more diverse group of electrodes based on porous metal structures, metal meshes, and metal-based woven fabrics. This class of electrodes can be further subdivided into three modifications: The first modification can be characterized as monolithic silver membranes with pore diameters ranging from a few hundred nanometers to 5 µm (Figure 8c). They can be synthesized by dealloying heterogeneous Ag-Al alloys by immersion in hydrochloric acid[72,73] or purchased commercially.[32,151,152] The dealloying technique was described in detail by Lu et al.[153]

The second subclass is based on metal meshes and foams, which were used as substrates for the deposition of silver nano- and micromaterials (Figure 8d).[25,41,154] For example, a silver mesh can be used directly after activation by electrooxidation,[155] or Ag can be deposited onto Cu and Ni meshes by impregnation or electrodeposition.[58,64] Finally, silver-based catalyst inks with PTFE as the binder and methylcellulose as a coagulation inhibitor were airbrushed onto Ni meshes and treated by hot pressing and sintering to obtain a homogeneously micro-structured GDE with PTFE-covered silver grains.[31,102,103] The detailed methodology was described by Moussalem et al.[101]

Another modification can be denoted as silver hollow fibers, which were fabricated by preparing a slurry composed of silver particles and polyetherimide, which was treated by extrusion with a spinning device, forming in a water bath for phase inversion and subsequent calcination (Figure 8e).[30,59]

The third category can be defined as carbon-based GDEs and represents the electrode structure that is most used in

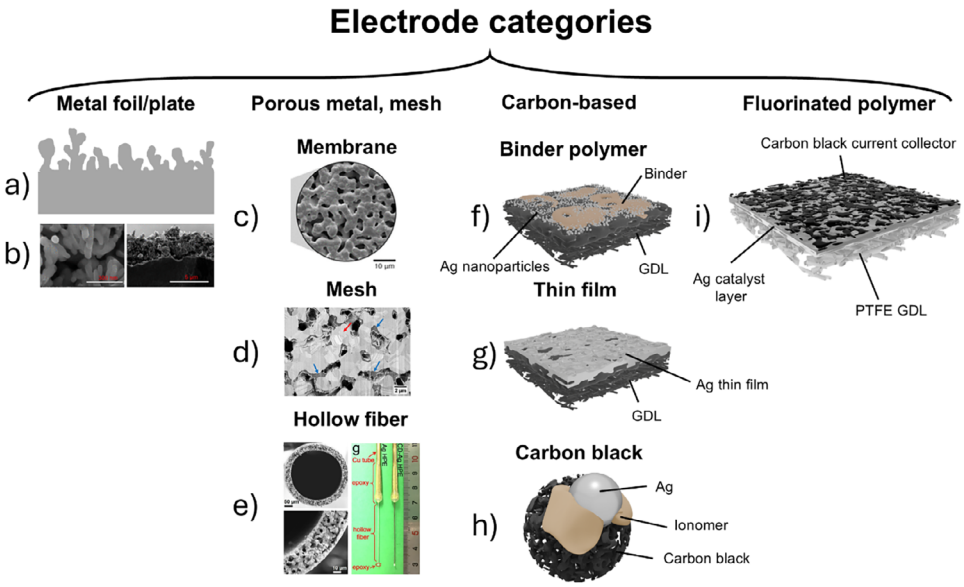

Figure 8. Schematic overview of the electrode structures used and modified in the literature dataset. Four main types are identified: Metal foils and plates used in H-type cells, porous metals, meshes or woven fabrics, carbon-based and fluorinated polymer membrane-based GDEs: a) Schematic representation of surface modified Ag foil, reproduced from ref. [156]. b) Scanning electron microscopy (SEM) image of modified Ag foil surface,[157] c) SEM image of a commercial silver membrane,[32] d) Focused ion beam (FIB)-SEM image of silver GDE based on Ni mesh,[158] e) SEM image and photograph of Ag hollow fiber electrode,[59,159] f) Schematic representation of a GDE based on binder-coated silver nanoparticles, reproduced from ref. [54]. g) Scheme of a GDE with a thin Ag catalyst layer, reproduced from ref. [160]. h) Scheme of ionomer-bound silver nanoparticles on carbon black particle, reproduced from ref. [161]. i) Silver GDE based on PTFE membrane. reproduced from.[33] Reprinted with permission from cited references (b,c,d). Reproduced under terms of the CC-BY license (e).

low-temperature CO_2 electrolysis (see Figure 3). It is typically based on the combination of three building blocks: A carbon fiber substrate, often referred to as the carbon fiber layer (CFL) or a macroporous substrate (MPS), which serves as the GDL; a microporous layer (MPL), and the catalyst layer itself. Both layers may contain hydrophobic binders, such as polytetrafluoroethylene (PTFE), to increase the hydrophobicity and thus decrease the selectivity toward hydrogen evolution.[76,81,162] Within the dataset, the GDL was prepared in-house in three studies only, while in most studies, commercially available gas diffusion substrates were used.[66,76,163]

Accordingly, we do not focus on modifications of the GDL or microporous layer (e.g., content of hydrophobic agent, permeability, woven or nonwoven, etc.) to subdivide the broad class of carbon-based GDEs. Instead, structural modifications of the catalyst layer that was deposited on top of the carbon support are considered.

In the dataset, three subgroups of carbon-based GDEs can be defined. The most commonly used structure was prepared by ink-based methods using Ag nanoparticles in combination with a binder polymer (both ionic and non-ionic, such as PTFE) to obtain a homogeneous catalyst layer (Figure 8f). The catalyst layer can be thought of as a distribution of silver nanoparticles coated with or embedded in the binder polymer.[17,18,20,24,45,51,52,54–57,76,78–81,83,85,86,90,93,97,99,100,162–183]

The binder materials applied in the literature dataset are reported in **Figure 9**, which shows that Nafion was most frequently used for ink preparation and to bind the catalyst to the GDL. Furthermore, Sustainion, PTFE, and Piperion binders were also used. The frequent use of perfluoroalkyl substances (PFAS) in the catalyst layer (e.g., Nafion, PTFE) but also in the MPL of most carbon GDLs (e.g., PTFE) is problematic considering their toxicity and bioaccumulation properties. In its 2020 Chemical Strategy for Sustainability, the European Commission has proposed a ban on PFAS in applications that are not considered "essential for society".[184,185] Correspondingly, it may be anticipated that future restrictions also affect Nafion and PTFE for Ag-based GDEs, which necessitates the development of alternatives. Recent studies comparing binding agents in the catalyst layer have shown that fluorine-free binders like Sustainion, PiperION, or Fumion can achieve comparable performance at low current densities.[27,48,83,186] Furthermore, a current density of 1004 mA cm^{-2} for CO formation was achieved with PiperION employed as a binder by Endrődi et al.[39] Von Tettau et al.

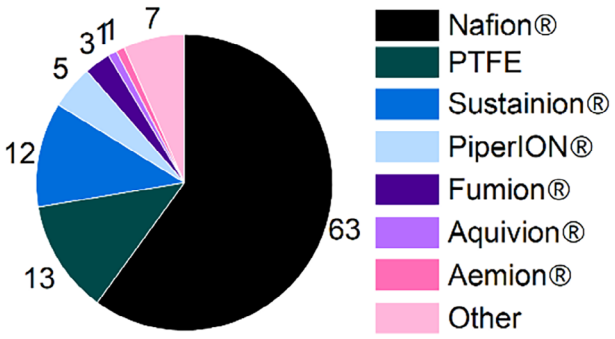

Figure 9. Binder polymer materials used in the catalyst layer as derived from the analyzed literature dataset.

propose partially fluorinated polymers like polyvinylidene fluoride and polyfluoropolyethers or silicone materials as an alternative to PTFE in the GDL, albeit for PEM MEAs, which can certainly be transferred to eCO_2R systems.[187]

The second sub-group introduces the application of the catalyst without a binder polymer, typically performed via electrodeposition or physical vapor deposition methods to obtain a thin film of silver on the GDL surface (Figure 8g).[19,50,61–63,188–197]

While the first two subgroups represent electrode structures with a rather smooth catalyst surface, the last subgroup is based on the incorporation of carbon black powder as a catalyst support for silver nanoparticles in order to increase the active surface area of the catalyst material (Figure 8h). Typically, the carbon black was first mixed with the silver nanoparticles to obtain a supported catalyst, which was then applied to the GDL.[6,22,26,48,49,82,84,94,96,98,198–210] The surface-enhancing effect was also exploited by using carbon nanotubes as a catalyst support.[77,211]

The final category identifies GDEs based on fluorinated polymer membranes (mainly PTFE, but also polyvinylidene fluoride (PVDF)), which act as a GDL (Figure 8i). The typical preparation method for PTFE-based GDEs was introduced by Dinh et al. with two objectives: To avoid flooding that occurs in carbon-based GDLs and to decouple the current flux and CO_2 mass transport pathways. Accordingly, a sputtered Ag catalyst layer was sandwiched between a PTFE membrane as the GDL and a sprayed carbon black layer as a current collector.[33] Similar multilayer structures, including the substitution of carbon nanotubes for carbon black or electrodeposited instead of sputtered Ag catalyst layers, were applied by other authors.[212–220]

2.4. Performance Analysis

In this section, the performance of the above classified electrode structures/substrate types is evaluated. The maximum reported partial current density for carbon monoxide formation, max. j(CO), and the duration as well as the applied partial current density for CO generation in extended laboratory experiments were extracted either from plots (visual observation) or from reported values.

Figure 10a,b shows the maximum reported j(CO) as a function of the electrode substrate and the cell type/test environment, respectively. The average reported max. j(CO) (square) was in the same range for carbon-based, porous metal-based, and fluorinated polymer membrane-based GDEs, 231, 181, and 245 mA cm^{-2}, respectively. For metal foils or plates, the max. reported current density did not exceed 65 mA cm^{-2}, which is in good agreement with the limiting current density for CO_2 electroreduction to CO in aqueous systems based on the semi-infinite diffusion model, i.e., ≈60 mA cm^{-2}.[221,222] The four data points corresponding to an electrode structure that could not be assigned to any of the four classes were in the range of 0–200 mA cm^{-2} and thus do not compete with the performance of the three GDE groups.

Despite the similar average max. j(CO) of the three GDE groups, only in the studies with carbon-based GDEs, current densities of 500–700 mA cm^{-2} were also reported.[39,54,80,97–99,162,223,224] Furthermore, one of the two highest partial current densities for CO formation in the analyzed dataset, i.e., 1004 mA cm^{-2}, was achieved with a carbon-based GDE by Endrődi et al.[39] A similar max. j(CO) of ≈1000 mA cm^{-2} was achieved in the dataset with a GDE based on a PTFE membrane, as reported by Edwards et al. The group sputtered a 500 nm thick Ag layer onto the PTFE membrane and sprayed a Nafion-bound carbon black layer on top.[220]

Figure 10b shows the same data regarding max. j(CO) as a function of the cell type employed. As expected for H-cell studies, in most publications, current densities did not exceed 100 mA cm^{-2}. In five studies, current densities between 100 and 300 mA cm^{-2} were reported, which can be explained by the use of GDEs, which were mainly operated in flow-through mode using an H-cell setup.[30,58–60,64] The average reported max. j(CO) for the three cell types that typically employ a GDE, the conventional GDE setup cells, the zero-gap cells, and the MEA cells were 266, 374, and 222 mA cm^{-2}, respectively. An evaluation of the three cell types in terms of their performance based on the data should be treated with caution, because the cell types were tested under different experimental conditions, e.g., electrolyte composition, feed rate, etc.

In Figure 10c,d, the extracted data on the duration of the extended laboratory electrolysis experiments and the corresponding partial current density of CO, j(CO), in these experiments, are shown. Note that the partial current density for CO formation at the end of the extended electrolysis experiment was considered, e.g., in a galvanostatic experiment with a total current density of 100 mA cm^{-2}, with decreasing FE(CO) from 95% to 60%, 60 mA cm^{-2} was considered as j(CO). The average reported partial current density for the CO formation at the end of the stability tests was 134, 130, and 143 mA cm^{-2} for the carbon-based, metal-based, and fluorinated polymer-based electrodes, respectively. Stability tests for electrodes based on metal foils and plates were performed at much lower current densities (average j(CO) 7 mA cm^{-2}). On the other hand, the duration of the extended laboratory experiments varied between the three classes of GDEs. For carbon-based, porous metal-based, and fluorinated polymer-based GDEs, the average reported duration of the stability experiments was 181, 442, and 45 h, respectively. At the same time, the two longest laboratory experiments in the analyzed dataset, i.e., 4380 h reported by Kutz et al. and 3800 h reported by Liu et al., were performed using a carbon-based GDE.[93,94] The stability of GDEs is discussed in more detail in Section 3. In Figure 10d, the same stability data were resolved as a function of the cell type employed. The average partial current density for the formation of CO for the three cell types that typically employ GDEs (conventional GDE, zero-gap, and MEA designs) was 128, 226, and 157 mA cm^{-2}, respectively. At the same time, the average reported duration of the stability experiments was 154, 16, and 413 h, respectively (for conventional GDE, zero-gap, and MEA designs). Accordingly, while the zero-gap design was tested at higher current densities on average, the duration of the reported stability experiment was shorter compared to the conventional GDE design and the MEA design. On the other hand, the H-cell configuration was only tested at lower current densities and shorter electrolysis durations. The analysis shows that all three identified GDE categories are promising

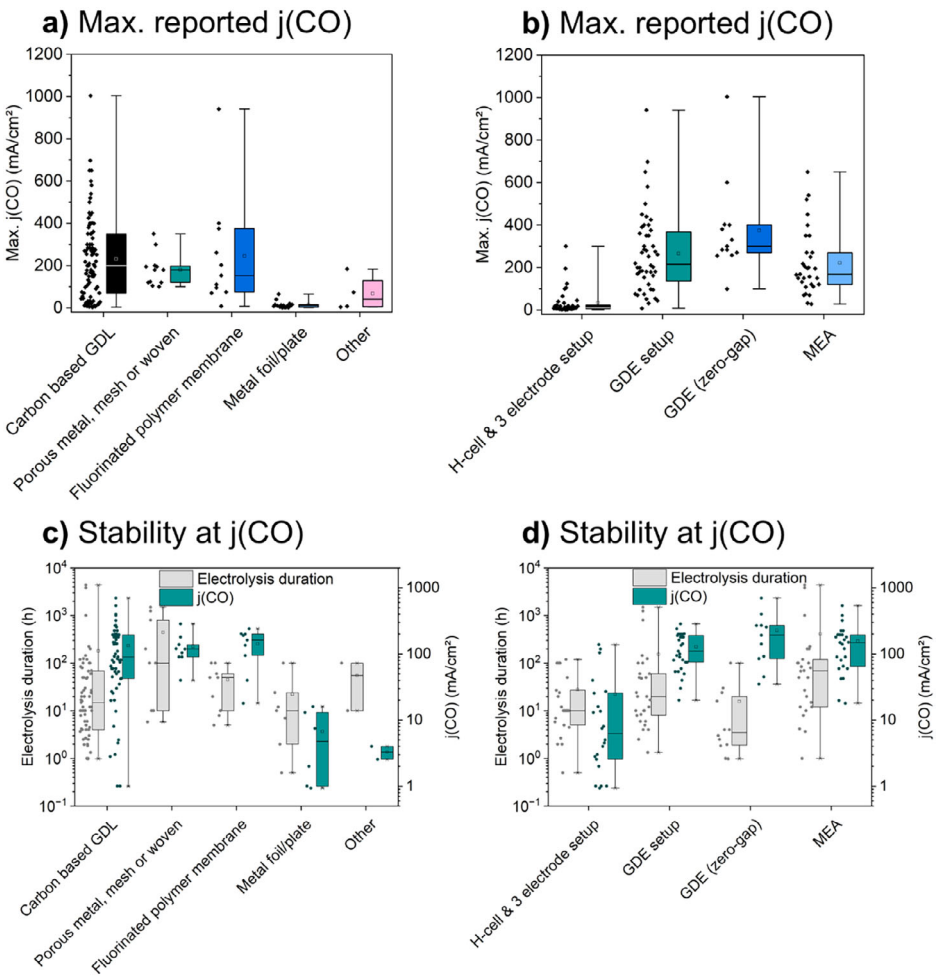

Figure 10. Performance analysis of the literature-based CO_2 electrolysis dataset, including only studies in which Ag-based electrocatalysts were used. Both original scatterplot data (left) and box plots (right) are shown for each entry. Note that for each box plot, the line indicates the median, the square indicates the mean, the box indicates the 25–75% percentile, and the whiskers indicate the min/max range. a) Maximum reported partial current density for carbon monoxide formation, j(CO), as a function of electrode substrate. b) Maximum j(CO) as a function of cell type. c) Duration of long-term experiments and j(CO) at the end of the experiment as a function of electrode substrate. d) Duration of long-term experiments and j(CO) at the end of the experiment as a function of cell type.

candidates for low-temperature CO_2 electrolysis based on the reported maximum. j(CO) and stability. Nevertheless, the longest operation of CO_2 electrolysis was reported with carbon-based GDEs.

For the commercialization of the low-temperature electrolysis of CO_2, techno-economic analyses suggested that a current density of 200–300 mA cm^{-2} must be exceeded.[225,226] In the recent techno-economic analysis by Shin et al., it was pointed out that higher current densities in the range of 300–700 mA cm^{-2} can significantly reduce the production cost of carbon monoxide and other reduction products.[110]

CO_2 electrolysis at higher current density has been achieved only recently.[15] **Table 2** summarizes the studies in the literature dataset in which partial current densities for carbon monoxide formation above 500 mA cm^{-2} were reported. In addition, three studies have been added that were not found in the Web of Science search due to different topics and abstract specifications, and/or terminology.[159,227,228]

2.5. Structure-Activity Relationships and Learnings from in situ and *in operando* Characterizations

In the following section, structure-activity relationships concerning electrocatalyst and electrode properties in the context of silver-based GDEs are discussed, as well as key findings from recent in situ and *in operando* studies. The authors emphasize that this discussion is by no means exhaustive. Therefore, readers interested in in-depth insights, e.g., discussions regarding reaction mechanisms, are referred to published works, such as review articles that describe the state of the art in those fields.[229,230]

Structure-activity relationships for the Ag-based electroreduction of CO_2 have been reported on different scales of the (gas diffusion) electrode as given in **Table 3**.

Silver-based catalysts are highly selective and enable low kinetic overpotentials for CO_2 to CO conversion compared to other metals. Based on a study carried out with well-defined surface

Table 2. Studies featuring partial current densities for the formation of CO, j(CO) > 500 mA cm^{-2} on silver-based GDEs. Except for the studies by Edwards et al. (50 bar), Endrődi et al. (60 °C), Samu et al. (60 °C), and Sun et al. (55 °C), electrolysis experiments were performed at ambient pressure and temperature, or experimental conditions were not specified.

Author	Cell type	j(CO) [mA cm^{-2}]	FE(CO) [%]	Catholyte	Electrode structure	Refs.
Li et al.	H-cell (Flow-through)	4300	95	3 M KCl + 0.05 M H_2SO_4	Porous metal (Ag hollow fiber)	[159]
Wen et al.	FTDT cell	≈2970	88	0.5 M $KHCO_3$	Carbon-based	[227]
Li et al.	GDE setup	≈1080	≈90	1 M KOH	Carbon-based	[228]
Endrődi et al.	Zero-gap	1004	≈91	–	Carbon-based	[39]
Edwards et al.	GDE setup	941	≈60	5 M KOH	Fluorinated polymer membrane	[220]
Chen et al.	GDE setup	≈700	≈93	1 M KOH	Carbon-based	[97]
Samu et al.	MEA	≈650	≈96	–	Carbon-based	[162]
Zhang et al.	GDE setup	≈650	–	4 M KCl (pH = 2)	Carbon-based	[223]
de Jesus Gálvez-Vázquez et al.	Zero-gap	≈600	70	–	Carbon-based	[98]
Bhargava et al.	GDE setup	≈580	≈100	2 M KOH	Carbon-based	[80]
Du et al.	MEA	≈540	≈90	–	Carbon-based	[54]
Sun et al.	MEA	≈520	≈75	–	Carbon-based	[224]
Zhang et al.	GDE setup	≈500	≈90	1 M KOH	Carbon-based	[99]

structures enabled by Ag-coated single-crystal Si wafers, it was found that an Ag(110) thin film performs more favorably relative to Ag(100) or Ag(111), as evidenced by an increased partial CO current density.[231] This was rationalized by the surface steps being more active than more highly coordinated terraces, which was supported by DFT calculations.

A higher binding energy achieved with the Ag(110) surface structure with respect to the important intermediate *COOH, in concert with an enhanced double-layer electric field stabilization over undercoordinated surface atoms located at step edge defects, are the main factors. Beyond metallic nanoparticulate silver, silver-based single-atom catalysts enable the engineering of the active site on the atomic level. For instance, Ag single atoms have been coordinated with polyaniline, forming the anchoring sites.[232]

The amino group (—NH—) of the polymer exhibits a strong electron donation ability, which favors the electron transfers during CO_2 reduction. Further, this functional group improves the CO_2 activation and the adsorption of *COOH. Both factors contributed to superior selectivity compared to a silver-based GDE with no polyaniline modification (≈100% vs ≈54% at −0.75 V vs RHE).

Significant research efforts have been allocated in recent years to the surface modification of metallic silver catalysts with the

Table 3. Structure-activity relationships on different scales of Ag-based (gas diffusion) electrodes.

Scale	Study	Structure-activity relationship
Catalyst	Clark et al.[231] (2019)	Increased CO partial current density for Ag(110) compared to Ag(100) and Ag(111), rationalized by higher binding affinity and electric field stabilization according to DFT calculations.
	Zhang et al.[232] (2024)	Ag single atom catalyst coordinated by polyaniline-based anchoring sites: Electron donation of the amino-group facilitated electron transfer
Catalyst surface	Li et al.[228] (2025)	Integration of molecular indigo derivatives with redox-active CO_2 binding sites at the Ag catalyst interface significantly reduces the onset potential for CO_2 reduction to CO, which is rationalized by their synergistic complexation/activation of CO_2 and the resulting increased availability of $*CO_2^-$ and *COOH intermediates
	Abdinejad et al.[233] (2022)	Electrografted pyridines on Ag surfaces decrease the CO_2 reduction onset potential by ≈200 mV and increase the activity tenfold, which was rationalized by the CO_2 capture ability of the pyridines.
	Jiang et al.[183] (2017)	Bound O-atoms on Ag surface increase selectivity for CO production from ≈20% to 90% at ≈−0.95 V vs RHE. High electron affinity of the O-atoms: Reduction of electron density at Ag sites, favoring $*CO_2^-$ adsorption.
Reaction environment	Ko et al.[234] (2024)	Oleylamine: Reduction of water volume fraction in GDE during operation
	Du et al.[54] (2022)	Catalyst particles coated uniformly with ionomer (synthesis of Ag nanoparticles with co-dissolved ionomer) significantly outperformed GDEs based on ultrasonicated mixtures of Ag and ionomer.
MPL	Wu et al.[6] (2022)	Low current densities: Thin MPL is advantageous for CO_2 mass transport. High current densities: Thick MPL is advantageous for flooding resistance
CFL	Baumgartner et al.[81] (2022)	Broad bimodal pore size distribution is beneficial for diffusivity

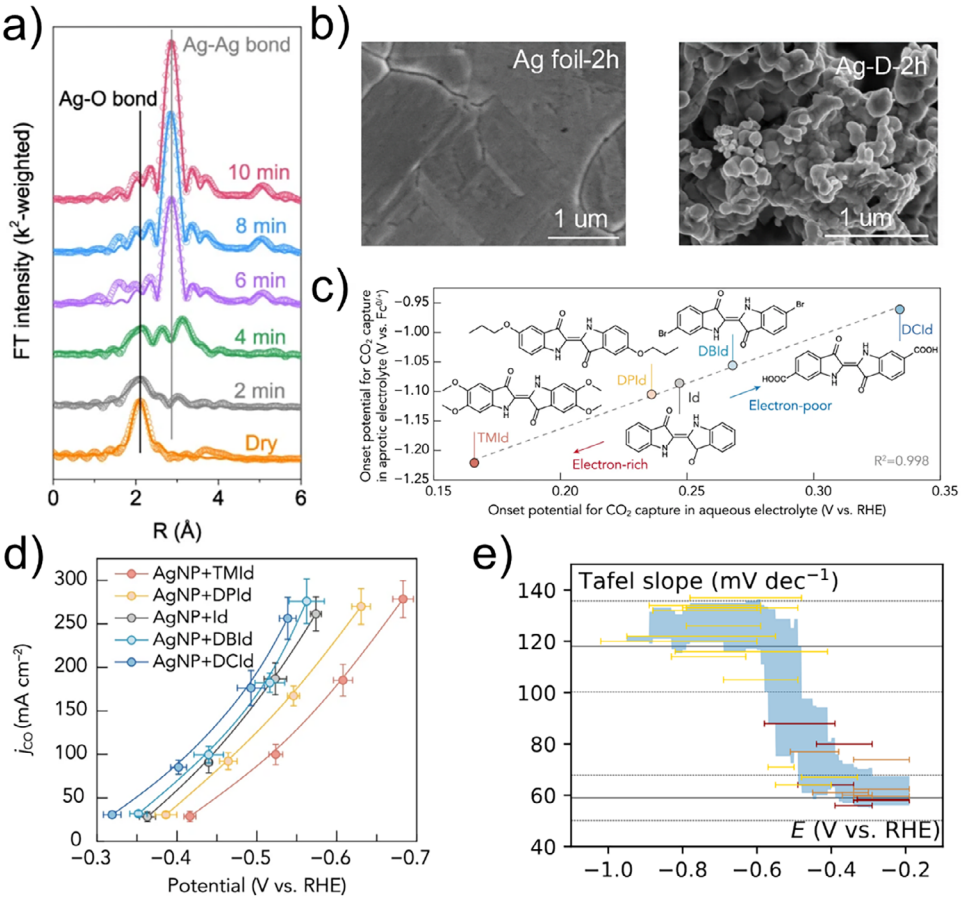

Figure 11. a) *In operando* Fourier transformed EXAFS spectra and fit of Ag_2O precatalyst termed Ag-D under electrolysis conditions. b) SEM images of Ag foil and Ag-D catalyst after 2 h electrolysis.[210] c) Linear relationship between the onset potential of CO_2 capture in aprotic and aqueous electrolyte for functionalized indigos. d) Activity of Ag nanoparticles modified with functionalized indigos.[228] e) Tafel slopes for CO_2 electroreduction on Ag surfaces[235] Reproduced under terms of the CC-BY (a,b,e) and CC-BY-NC-ND (c,d) license.

aim of tuning their electronic and structural properties in favor of CO_2 reduction.

Indigos (organic pigments) can be utilized through their electrochemical activation to intensify the activation of CO_2 and formation of key intermediates in conjunction with Ag nanoparticles (**Figure 11**c,d).[228] The resulting local surface environment leads to a bent configuration of the CO_2 molecule, which reduces the activation energy. Indigo derivatives withdraw electron density from adjacent Ag sites, reducing the overpotential for CO formation, which can be related to the onset potential for CO_2 capture. The adsorption energy was increased threefold with indigo-functionalized silver (from ≈−0.21 eV to ≈−0.64 eV), which reduces the energy required for activation of $*CO_2^-$. Compared to an unmodified Ag catalyst, there was a positive potential shift of ≈70 mV at 25 mA cm^{-2}, and ≈180 mV at 150 mA cm^{-2}, respectively. At current densities below 100 mA cm^{-2} the modified catalyst exhibited a Faradaic efficiency of roughly 95%, outperforming the reference sample by 5%. The modified catalyst upheld this level of performance at 200 mA cm^{-2}, whereas the plain silver yielded a drop in the Faradaic efficiency to ≈85%.

Electrografted pyridines on Ag were tested at current densities of up to 200 mA cm^{-2}. Pyridine was attached to the surface by way of electrografting utilizing diazonium salt chemistry.[233] A 200 mV shift of the onset potential was observed relative to the unmodified silver electrode, as well as a roughly ten times increased current density at −0.7 V vs RHE (≈0.3 to ≈3 mA cm^{-2}). The partial current density for the HER was consistently higher when the bare silver electrode was employed, particularly at higher current densities of 150–200 mA cm^{-2}. To fabricate the GDE, a thin Ag film was sputtered onto a GDL. A MEA-based single cell was run with 1 M KOH as the anolyte. Up to 50 mA cm^{-2}, the GDE modified by electrografting clearly performed better as indicated by a lower cell voltage. However, at 100 mA cm^{-2} and also at higher current densities, the cell voltage was not stable and started to drift, which also led to a reversal in performance, i.e., the unmodified electrode yielded a lower cell voltage at 200 mA cm^{-2}. Reaction mechanisms were explored by applying attenuated total reflectance surface-enhanced infrared absorption spectroscopy (ATR-SEIRAS) and DFT calculations. In the case of Ag with electrografted pyridine, an increased intensity in the peak corresponding to $*CO_2^-$ compared to bare Ag was measured, which was rationalized by their CO_2 capture ability.

The environment adjacent to the active sites is also very important. Here, the local distribution of ionomers or polymeric

binders is crucial to control the hydrophobicity of the catalyst surface. For instance, it was shown that the synthesis of Ag nanoparticles in the presence of co-dissolved ionomer results in uniformly coated catalyst nanoparticles, as supported by SEM and FIB-SEM imaging. By contrast, when the ionomer and Ag nanoparticles are only ultrasonicated after mixing, the ionomer tends to accumulate on the surface. In fact, electrochemical impedance spectroscopy (EIS) showed significantly higher charge transfer and diffusion resistance in the latter case. The GDE based on the uniformly coated Ag particles showed 90% Faradaic efficiency for CO compared to 45% obtained with the reference sample at 600 mA cm^{-2}.[54] The hydrophobicity of the catalyst layer can be tuned via functionalization with hydrophobic ligands like oleylamine.[234] In a recent study, it was found that the functionalization of Ag nanoparticles with oleylamine increased the GDE hydrophobicity under working potentials. Correspondingly, the volume fraction of water penetrating the GDE was significantly reduced, as indicated by in situ/*in operando* synchrotron computed tomographs.

With respect to electrode design, the key objective is to prevent flooding while allowing sufficient transport of CO_2 to the active sites in the catalyst layer. Both depend on the structure of the gas diffusion layer, its hydrophobicity and thickness, as well as possible cracks, ultimately determining the location of the triple phase boundary.[236,237] GDEs can only be operated within a certain differential pressure window, and there is a trade-off between flooding resistance and mass transfer capabilities. The key component is the microporous layer between the catalyst layer and the GDL.[6] At relatively low current densities, a thin MPL leads to a higher concentration of CO_2 in the catalyst, while a thick MPL improves flooding resistance, which is key at high current densities. With respect to the fibrous structure of the gas diffusion layer, one study revealed that a broad bimodal pore size distribution is advantageous, with small pores (10 µm) between individual fibers and large pores (85 µm) between fiber bundles. This bimodal distribution is beneficial for reactant diffusivity.[81]

Recently, cell designs and spectroscopic and microscopic techniques have been successfully adapted to enable in situ and *in operando* investigations of the electroreduction of CO_2, in part also up to high current densities, as summarized in **Table 4** with the respective key findings of each study. The applied techniques include electrochemical impedance spectroscopy, microscopic techniques like electrochemical atomic force microscopy (EC-AFM) and confocal fluorescence microscopy (CFM), and spectroscopic techniques like X-ray absorption spectroscopy (XAS), a series of infrared-based techniques (see list of abbreviations), Raman spectroscopy (RS), and nuclear magnetic resonance spectroscopy (NMR).

As an example for microscopy techniques, Nesbitt and Smith have used *in operando* EC-AFM measurements to monitor Cu and Ag GDEs at −100 mA cm^{-2}, finding that the topography is stable under the operating conditions tested.[197] Welch et al. were able to show that the local pH in the cracks of catalyst-coated GDLs is significantly higher compared to surface values by applying *in operando* CFM.[238]

Using *in operando* Fast XAS Wu et al.[210] observed the structure evolution of an Ag_2O precatalyst during CO_2 reduction. The transient Extended X-ray Absorption Fine Structure spectra (EXAFS) shown in Figure 11a indicated the reduction to metallic Ag. In Figure 11b, SEM images of Ag foil and the in situ formed Ag catalyst termed Ag-D are shown, each after 2 h of electrolysis. Analysis of the coordination number (CN) by fitting the EXAFS spectra revealed a significantly lower CN for the Ag-D catalyst (≈7.2) compared to the CN in Ag foil (12) after 30 min, which was interpreted as a high defect concentration. Accordingly, the high defect concentration was linked to the superior performance.

Despite approaching industrially relevant performance data, CO_2 electroreduction on Ag surfaces is not yet fully understood on a mechanistic level. Boutin and Haussener have conducted a meta-analysis of published data on in situ infrared spectroscopy, Tafel slopes, and kinetic isotope effects to investigate the rate-determining step of the electrochemical reduction of CO_2 on Ag surfaces.[235] After analyzing 28 in situ infrared spectroscopy studies, they conclude that the reaction of the surface intermediate $*CO_2^-$ is very unlikely to be the limiting step. The surface species have not been detected, except in one study, where the authors indicate confusion was likely. Instead, based on the Tafel slope (≈120 mV dec^{-1}) at potentials lower than −0.6 V vs RHE (Figure 13e) significant evidence was found for the one-electron transfer to CO_2 being the rate-limiting step. This is also in agreement with the absence of any kinetic isotope effect when deuterated water was used and the observed zero-order reaction for H^+ and HCO_3^-. Nonetheless, the question of why the Tafel slope decreases to ≈60 mV dec^{-1} for potentials higher than −0.4 V vs RHE is still unanswered, demanding further research.

In situ and *in operando* spectroscopy and microscopy techniques can provide a deeper understanding of catalyst structure development, local variations of activity, and underlying mechanistic principles.[239]

Furthermore, a correlative approach linking different characterization techniques can help in deciphering underlying structure-activity relationships.[210] Nonetheless, cell designs have to be significantly modified to enable these characterizations, possibly imposing different local conditions compared to cells designed to produce CO for customers.

The systematic literature review presented in this work shows that ink-based methods are the standard technique for the preparation of silver-based GDEs. Two main problems have been identified with the current methods: First, a high catalyst loss during the preparation process is often reported (Figure 7).

Therefore, it should not only be the aim to minimize the catalyst loading on the electrode itself, but also to minimize the catalyst waste during the preparation of the GDE. Second, a significant mismatch between the ink and catalyst composition was identified, which is problematic as the composition of the catalyst layer was usually not analyzed (Figure 6). Most likely, the different agglomeration and sedimentation tendencies of the ionomer and the Ag nanoparticles resulted in deviations between the catalyst ink and the catalyst layer composition.[87–89] Since these deviations depend on the experimental methodology, it is strongly recommended to report the experimental details of the ink-based methods. Despite the excellent intrinsic activity and selectivity of Ag itself, recent studies investigating structure-activity relationships showed that there is still room for optimization of Ag active sites. The surface modification with moieties able to electrochemically capture CO_2, e.g., indigos and pyridines, has shown promising activity and selectivity improvements. These interfacial design strategies not only affect the electrode performance

Table 4. In situ and *in operando* studies on CO_2 electroreduction using different techniques and the corresponding key findings. For technique abbreviations, see the list of abbreviations.

Study	Technique(s)	Electrochemical performance	Key findings
Bienen et al.[240] (2020)	*In operando* EIS	Sn GDE, −125 mA cm^{-2}, 82%FE($HCOO^-$)	The impedance spectrum corresponds to four processes: Ionic and electrical conductivity of the porous electrode, hydroxylation of CO_2, electron transfer to CO_2, and CO_2 diffusion.
Nesbitt & Smith[197] (2021)	*In operando* EC-AFM	Cu and Ag GDEs, −100 mA cm^{-2}	Demonstration of cell design supporting EC-AFM for high current densities. Topography is stable up to −100 mA cm^{-2}
Welch et al.[238] (2021)	*In operando* CFM	Cu GDE, −28 mA cm^{-2}	Variations of pH across the surface indicate local variation of activity. pH increases in the cracks of the catalyst-coated GDL
Wu et al.[210] (2021)	*In operando* Fast XAS	Ag_2O precatalyst	Monitoring of the structure evolution of Ag_2O precatalyst: X-ray spectrum indicates reduction to metallic Ag, however, with significant defect concentration indicated by the coordination number, resulting in a highly active catalyst
Firet et al.[241] (2020)	*In operando* XAS	Ag, Cu GDEs, −200 mA cm^{-2}	No pronounced difference in crystallite size and coordination number of Cu between −100 and −200 mA cm^{-2} indicating that a change in product selectivity is not connected to catalyst restructuring but a change in reaction environment
Boutin & Haussener[235] (2024)	In situ IRRAS, SEIRAS, ATR-FTIR, SERS	Ag electrodes	Meta-Analysis of Tafel slopes and intermediates for CO_2 reduction to CO. Most likely, the electron transfer to form CO_2^- is the rate-limiting step for potentials <−0.6 V vs RHE
Lu et al.[242] (2020)	In situ RS	CoPc GDE, −150 mA cm^{-2}	Reaction of CO_2 with produced OH^- at the cathode interface results in a pH profile spanning ≈10–100 µm, depending on the current density
Jovanovic et al.[243] (2023)	*In operando* NMR	Ag electrodes −10 µA cm^{-2}	^{13}C, ^{23}Na spectra to investigate electrolyte chemistry: Two distinct peaks for ^{13}C in HCO_3^- and ^{23}Na corresponding to free ions and ion pairs. CO_2/HCO_3^- equilibrium kinetics accelerate with increasing potential due to longer lifetimes of ion pairs in which Na^+ can stabilize the intermediate $H_2CO_3^+$. The impact of the electric field extends significantly into the bulk.

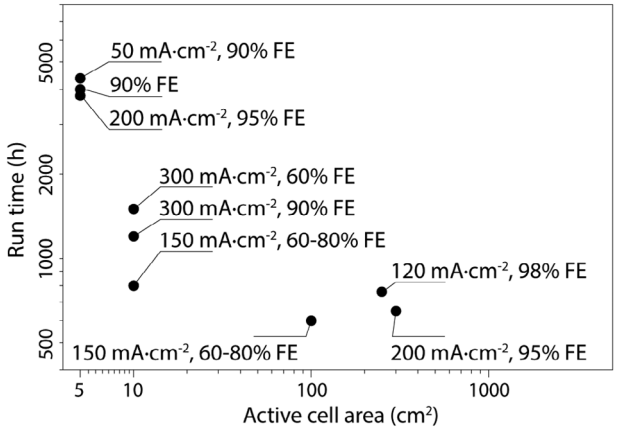

Figure 12. Overview of long-term operation studies as a function of active cell area. Publications with t < 500 h were excluded. Based on reported data by Liu et al.,[94] Kaczur et al.,[244] Kutz et al.,[93] Haas et al.,[74] Krause et al.[41] and Jeanty et al.[25]

but are also directly tied to the feasibility of moving the electrode design from the lab to the industrial scale. Whereas the indigo-based modification relied on ultrasonic mixing and spray coating -methods compatible with scale-up- the electrografting-based modification involved diazotization and electrochemical reduction, processes that are less easily adapted to large-scale manufacturing.[228,233] Correspondingly, for large-scale fabrication, the cost of introducing these moieties (electrografting, synthesis of promoting polymers, etc.), their compatibility with continuous manufacturing processes, and also their long-term stability will mainly determine their suitability for future application. To provide more detailed information, studies reporting on extended operating times are discussed in the following section.

3. Long-Term Operation Studies, Scale-Up, and Stack Development

Most published experiments related to silver-based GDE development and testing at the lab scale lasted several hours at most. It is important to study the long-term behavior of such electrodes in full cell experiments to be able to predict the lifetime and to better understand degradation phenomena. Extended operating times were reported by Haas et al. (1200 h, cell voltage 7–7.5 V,[74]) and Krause et al. (1500 h, cell voltage ≈7 V,[41]), and the Faradaic efficiencies at 300 mA cm^{-2} were 60% and 90%, respectively, with 10 cm^2 cells. Long-term operation studies are summarized in **Figure 12**.

A high CO selectivity of 95–98% was reported for a 5 cm^2 cell, which ran continuously over 3800 h at 200 mA cm^{-2}.[94] The corresponding voltage increase over time was 3 μV h^{-1}. The authors emphasized that water management was crucial to achieve an extended lifetime, and that this requirement could not be met by simply feeding humidified carbon dioxide to the cell. Other notable works yielded operation times of 4000 h and 4380 h, respectively, at ≈3 V with a Faradaic efficiency of 90% using anion exchange membranes from Sustainion.[93,244]

While considerable advances in long-term testing have been achieved in recent years, far greater operating life times are required for commercialization, e.g., stable performance over 100 000 h was stated as being highly desirable in the literature.[245]

Very few studies focus on degradation or cell failure mechanisms, salt precipitation aside. In particular, post-mortem characterization compared with pristine samples, which would offer valuable insights, is often missing in published studies. Microscopic imaging combined with spectroscopy and X-ray analysis would aid in revealing changes in the electrode structure and composition. Larger electrodes could be divided post-test and measured in smaller cells to detect possible variations in electrochemical performance due to locally varying degrees of degradation. The most common degradation cause is the formation of salt deposits from the electrolyte due to parts of the electrode drying out.[25] Analyzing impedance spectra and the concomitant distribution of relaxation times coupled with post-mortem characterization was demonstrated as a valuable tool to characterize the degradation behavior during long-term operation, albeit for a formate-producing system.[246] For instance, salt precipitation and restorative flushing could be monitored by impedance measurements.

It is crucial to demonstrate that improvements achieved at the lab scale can be transferred to commercially relevant cell dimensions. For example, with respect to PEM electrolysis, an active MEA area of 6000 cm^2 was estimated for a commercially manufactured system, i.e., the Silyzer 300 made by Siemens Energy.[247] Consequently, a similar scale is ultimately targeted for CO_2 electrolysis.

Siemens Energy reported a scale-up effort from 10 to 100 cm^2, i.e., constant current operation at 150 mA cm^{-2} was demonstrated over roughly 800 h and 600 h, respectively, while the Faradaic efficiency for CO varied between 60% and 80%.[25] A similar scaling step, i.e., from 8 to 100 cm^2, was realized by Endrődi et al.[39] At the smaller cell scale, the highest partial current density for CO production was achieved at 60 °C, after exploring the temperature range from 40 to 70 °C. In contrast, the partial current density for H_2 increased steadily with temperature. The highest partial current density for CO observed with the 8 and 10 cm^2 cell was ≈1000 mA cm^{-2}. A cell with an active area of 250 cm^2 performed reliably for 760 h at 120 mA cm^{-2}.[244] Under these conditions, the cell voltage varied between 2.9 and 3.05 V. The Faradaic efficiency with respect to CO ranged from 97.5% to ≈99%.

Bridging the gap toward industrially relevant cell dimensions, a stack consisting of ten cells with an active geometric area of 300 cm^2 each, also developed by Siemens Energy, was operated with the objective of direct utilization of the product gas in a bio-reactor.[248] In this configuration, a single cell maintained a Faradaic efficiency above 90% over a span of 200 h, and the corresponding stack continuously produced a stream with 30% $_{vol}$ CO over the same time period. Further, Krause et al. demonstrated a Faradaic efficiency of 95% at 200 mA cm^{-2} over 650 h with an analogous single 300 cm^2 cell, which included a shut-down and restart without affecting the cell performance.[41]

Operating electrolyzer stacks decreases the capital investment cost, as the scope of the balance of plant components is significantly reduced compared to running several single cells in parallel. Ideally, a multi-layer stack fits a larger number of cells with bipolar plates in between, and thus only two end plates are

required. Endrődi et al. showed that employing a stack with three cells connected in series improved the overall CO_2 conversion efficiency compared to operating in single cell mode.[40] At a CO_2 feed rate of 500 cm^3 min^{-1} the CO_2 conversion doubled (≈30% as opposed to ≈15%). In general, increasing the gas feed rate resulted in a more pronounced increase in conversion relative to single cell operation. On the other hand, an investigation of three cells set up in parallel did not yield a significant deviation from the performance of a single cell in this respect, as was observed consistently by applying three different cell voltages, i.e., 2.5, 2.75, and 3 V.

Quentmeier et al. demonstrated the absence of significant fluctuations in cell performance by investigating a short stack consisting of three cells, each with an active geometric area of 10 cm^2.[249]

Studies by Nelson et al. and Edwards et al. demonstrated the scale-up from 5 to 800 cm^2 and the development of a ten-cell stack at the 800 cm^2 cell scale.[250,251] Their focus was on converting CO_2 to ethylene using GDEs with a copper-based catalyst. Conceivably, some of the key findings from those works can be transferred to silver-based GDEs and the cells in which they are operated. It was found that nonuniformities in the electrode compression must be eliminated, and that the availability of sufficient CO_2 must be ensured across the entire electrode area to utilize the active sites as effectively as possible. Narrowing gas flow channels increased the pressure drop and thus enabled a more uniform distribution of CO_2. The Faradaic efficiency for ethylene was consistently increased at the 800 cm^2 scale compared to the laboratory scale cell when considering current densities of up to 100 mA cm^{-2}.[250] At higher current densities, this trend was reversed.

Pressurized operation improved the Faradaic efficiency of CO_2 to CO electrolysis[40] and is generally valuable from an operational cost perspective, as the product gas must be stored in a pressurized state for transportation, or downstream processes utilize the electrolyzer product gas at above-atmospheric pressure. In both cases, operating the electrolyzer under pressure could replace or at least alleviate the requirements for a compression unit that would be placed downstream of the cell(s) or stack. With respect to scale-up and long-term operation, the stability of the GDE, which strongly depends on the selected materials and the applied preparation technique, is one of the key parameters. In the following section, preparation techniques are compared in terms of their scalability.

4. Comparison of Electrode Fabrication Methods

At the laboratory scale, at which the active electrode area rarely exceeds 10 cm^2, the choices of electrode fabrication methods are manifold. Manual techniques, such as painting, brushing, drop-casting, or using a handheld airbrush, are common practice for carrying out the electrode preparation for laboratory work, but cannot necessarily be transferred to a manufacturing line, and especially not to larger electrode areas.[55,57,64,183] These techniques also inherently suffer from a low degree of reproducibility. In-plane uniform catalyst particle and ionomer distribution and a low degree of particle agglomeration are crucial for the electrode performance, ensuring a high active area and preventing the disruption of ionically conductive and electron transport pathways.[86] **Table 5** contains a comparison of electrode preparation techniques that are known from the literature.

Certain fabrication methods may lend themselves to semi-batch operating mode only, while others can be integrated into continuous processes. Shifting from hand painting to an automated airbrush process yielded a substantial improvement and a higher degree of reproducibility.[255] The latter observation was rationalized by a more pronounced variation of Ohmic losses because of a higher variance of the obtained catalyst layer thickness when hand painting was applied. Further, the Faradaic efficiency for CO was above 90% at potentials more negative than −1.5 V vs Ag/AgCl with the airbrush method, whereas hand painting yielded ≈80%. PVD methods are available to fabricate catalyst structures[33,62,256] and carbon-based materials,[257] which can, in principle, serve as catalyst support structures or GDLs. At present, such techniques are by and large limited to research activities in the field of electrochemistry, also because PVD methods inherently are applied to generate thin films or features (typically ≤1 µm). Electron beam physical vapor deposition was found to be superior compared to magnetron sputtering, albeit for copper-based GDEs, which were applied for ethylene production.[258] More specifically, an increased current density and (Faradaic) efficiency were obtained with the electron beam method, which was attributed to its benign effects with respect to the type of formed catalyst surface facets and a more defined interface between the catalyst layer and the GDL. Both PVD methods afforded GDE structures with a geometric area ranging from 25 to 600 cm^2, thus demonstrating the potential for scaling up. Generally, much of the experience gained from testing fabrication methods for PEMFC development, which spans several decades, can be exploited for electrode fabrication for CO_2 electrolysis processes. A direct comparison of applying either the doctor blade method or spray coating indicated that the latter improved the PEMFC performance by a factor of ≈2.9, based on comparing the measured current density at a defined cell voltage, i.e., 0.43 A cm^{-2} vs 0.15 A cm^{-2} at 0.6 V.[259] The authors attributed the performance gain through spray coating to the formation of mesopores due to a shorter drying time. The presence of mesopores enhances reactant access to the catalyst sites.

In this work, we focused on studies employing cells with either a liquid electrolyte gap between the cathode and the anode or MEA-based cells.

A GDE for oxygen reduction, prepared by spray coating, was modified to facilitate the conversion of CO_2 to CO.[253] The catalyst ink contained silver particles, a pore-forming compound, and PTFE. The substrate was a Ni mesh. While modifying the PTFE content did not yield satisfactory results, i.e., hydrogen evolution was the main reaction initially, reducing the pressure during the hot-pressing step from 160 to 100 bar allowed for an increase in the CO Faradaic efficiency from 27% to 59% at 25 mA cm^{-2}. By changing the Ag particle morphology and adjusting the electrode thickness, the Faradaic efficiency increased to 79%.

A continuous roll-to-roll process is most desirable, also from an operational cost perspective. A roll-to-roll redox coating process for alkaline water electrolysis electrodes was presented by Devi et al.[260] The coating speed was 4 cm min^{-1}, and high coating uniformity was demonstrated by nearly matching polarization curves obtained with samples prepared from different positions of the original coated sample. Conceivably, a similar process

Table 5. Comparison of electrode preparation techniques and the performance of the corresponding GDEs in carbon dioxide electroreduction.

Preparation method	Substrate	Hot-pressed	Electrode area [cm^2]	J [mA cm^{-2}]	FE [%]	Refs.
Hand painting	Carbon paper	no	2	51	85	[57]
Manual airbrush	Carbon paper	no	10	400	80	[55]
Dip coating	Carbon paper	no	1	20	92	[183]
Impregnation	Nickel foam		4	100	96	[64]
Sputtering	PTFE membrane	no	1	120	93	[33]
Electron beam evaporation	Carbon paper	no	10	100	95	[62]
Electro-deposition	Carbon paper	yes	136	3	83	[252]
Spray coating	Ni or polyether ether ketone (PEEK) mesh	yes	5	100	79	[253]
Spray coating	PTFE	no	100	300	50	[254][a)]

[a)] Ethylene production.

could be adapted to carry out the electroless deposition of silver particles on a carbon-based GDL substrate.

Roll-to-roll coating processes were compared by Mauger et al., highlighting the importance of the ionomer distribution.[261] In case the GDE should be bonded to an anion exchange membrane, it is desirable to have a certain degree of ionomer segregation, which means a thin layer of the ionomer is formed on the electrode surface. It was found that spray coating multiple layers does not provide this feature. On the other hand, coating with a slot die or a Mayer rod yields thicker films and, in conjunction with a high evaporation rate, enables the desired ionomer segregation. Electrodeposition of Ag on a carbon GDL was realized with substrate areas of 25.5 and 136 cm^2, respectively.[252] Faradaic CO-efficiencies of ≈80% to 90% were achieved with both areas, and a preferred deposition current density of 0.83 mA cm^{-2} applied for 50 min was identified, as lower or higher current densities led to lower uniformity of the catalyst layer. In another work, it was claimed that electrodeposition is superior to manual methods, i.e., drop-casting. In this case, a metal organic framework (MOF) was applied layer by layer as a template on carbon cloth, followed by electrodeposition of Ag as part of the MOF, resulting in a high Faradaic efficiency of 96% at 300 mA cm^{-2}.[50]

Carbon-based GDLs consist of carbon fibers, which are typically produced from polyacrylonitrile, involving several thermal treatment steps, including pyrolysis. Such GDLs reached commercial maturity many years ago, and therefore, the current limitation for silver-based GDE lies in the integration of the silver-containing catalyst layer into the electrode structure as part of the manufacturing process.

As an alternative to carbon-based GDEs, PTFE-based structures offer inherent hydrophobicity to establish a stable CO_2/electrolyte interface.[262] Multi-layered structures with varying Ag:PTFE ratios and layer thicknesses can be achieved by, e.g., spraying, a doctor blade-based approach, or screen printing. As PTFE is non-conductive, auxiliary or modified conductor compounds can be integrated into the electrode to improve the performance. Micro-scale conductors integrated into the PTFE layer connected the catalyst layer with the current collector and also reduced the in-plane conduction path.[263] This was demonstrated for electrodes with a size of 50 cm^2. The implementation of such conductive compounds afforded a reduction of the cell voltage by up to 0.9 V. Non-uniform current distribution, which also can lead to a local variation of the electrochemically produced species, was mitigated by a novel current collector design, as shown by van Montfort et al., albeit with a copper catalyst layer and ethylene as the target product. Copper busbars were applied on top of the catalyst layer, enabling a more uniform current distribution, while it was shown that the electrochemical process was still confined to the catalyst layer.[264] Similarly, a current collector was placed on top of a copper oxide catalyst layer used for ethylene production, which included a scaling step from 5 to 100 cm^2 with respect to the geometric electrode area.[254] A sintered PTFE membrane was utilized as the GDL, and the catalyst was applied by spray-coating. A Faradaic efficiency of ≈50% was achieved for ethylene at 300 mA cm^{-2} with the 100 cm^2 cell. Both the Faradaic efficiency (especially for CO and H_2) and the cell voltage were similar when comparing the small cell with the large cell.

The large-scale production of catalyst nanoparticles is not at a mature level yet. Most reports on research works looking into the scale-up of nanoparticle synthesis describe the synthesis of batches well below 1 kg or suspensions of ≈1 liter in volume or less over the course of 24 h.[265] Therefore, further development of such processes is required. Catalyst-containing inks, slurries, or pastes must be sufficiently stable and compatible with all electrode fabrication processing steps. Demonstrating the production of catalyst materials at the kilogram scale and developing continuous and automated spray coating and roll-to-roll processes for electrode fabrication was recommended by Segets et al.[266]

High catalytic activity is a requirement for commercialization, but minimizing Ohmic losses and mass transport limitations are bigger challenges in comparison. The impact of achieving reductions of Ohmic and mass transfer limitations on cell efficiency will likely be much more significant than further reducing the kinetic overpotential, which is governed by the catalyst properties. Overall, with respect to large-scale manufacturing, it is crucial to implement stringent quality control measures, spanning from monitoring catalyst properties, such as particle size, to ink composition and properties (e.g., viscosity) and GDE parameters, such as the compositional homogeneity and the thickness of the catalyst layer. Ideally, such parameters will be monitored in-line and in real time as part of a robust manufacturing process. The

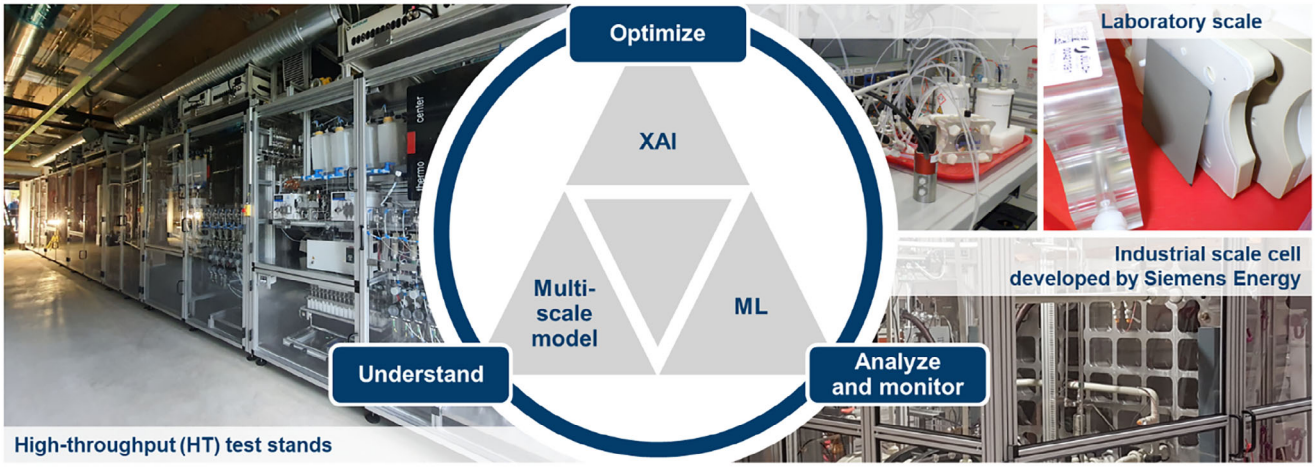

Figure 13. Schematic visualization of how different modeling approaches can contribute to monitoring, understanding, and optimizing experiments related to CO_2 reduction.

capability of models used to describe CO_2 electroreduction with GDEs will likely also affect the future optimization regarding transport limitations and the monitoring of the process, and is discussed in the following section.

5. Efforts on Modeling Multi-Scale and Multi-Physics Phenomena in GDEs

The electrochemical reduction of CO_2 is a complex multi-scale process involving simultaneous phenomena across different length and time scales.[267] This includes the interplay of macroscale mass transport and diffusion, atomic-level electron transfer, multiple reaction pathways with intermediate species, and ion migration through various components of the CO_2 electrolyzer, and especially GDEs. For CO_2 electrolyzers to be commercially viable, high current densities must be achieved with good selectivity at relatively low power inputs, as elaborated in Section 3. Achieving this performance necessitates careful design and optimization, which in turn requires a deep understanding of the underlying physics. This is where multi-scale and multi-physics modeling, as illustrated in **Figure 13**, becomes essential. Such physics-based approaches are implemented to simulate these systems using a coupled set of partial differential equations and to discretize these governing equations using techniques such as finite element[268] or finite volume methods.[269,270] **Table 6** contains a brief overview of the so-far published macro-scale physics-based models on CO_2 reduction to CO with silver-based GDEs. The software COMSOL Multiphysics is the most commonly applied one to implement macro-scale models.

Initially, Weng et al.[271] developed a 1D multi-physics model for CO_2 reduction at vapor-fed GDEs to explore the interplay between species transport and electrochemical kinetics. Their model showed how local conditions near the catalyst layer influence the cell performance. Additionally, they investigated the effects of catalyst layer hydrophobicity, loading, porosity, and electrolyte flow rate to provide insights for optimizing vapor-fed CO_2 reduction cells. Building on the need for accessible and broadly applicable modeling tools, Blake et al.[272] developed a simple and freely available analytical model of a cathodic catalyst layer configured to produce CO. Their work focused on elucidating the relationships between electrode reaction kinetics, cell operation conditions, catholyte composition, and cell performance. Analytical methods allowed them to cover parameter ranges, intractable for numerical and experimental studies.

More recently, Osiewacz et al.[102] advanced the field with a refined 1D mathematical model of a silver GDE for electrochemical

Table 6. Summary of the published models regarding CO_2 reduction to CO with silver-based GDEs. 1: COMSOL Multiphysics, 2: gPROMS ModelBuilder, 3: MATLAB.

Author	Year	Cell type	Membrane	Dimension	Software	Refs.
Lees et al.	2024	MEA	AEM	1D	1	[273]
Osiewacz et al.	2024	GDE setup	AEM	1D	2	[102]
Löffelholz et al.	2022	GDE setup	AEM	pseudo 2D	2	[274]
Blake et al.	2021	GDE setup	–	1D	1	[272]
Kas et al.	2021	GDE setup	PEM	2D	1	[275]
Kannan et al.	2019	GDE setup	–	2D	1/3	[276]
Weng et al.	2019	MEA	AEM	1D	1	[277]
Weng et al.	2018	GDE setup	AEM	1D	1	[271]

CO_2 reduction (eCO_2R). The 1D model, discretized along the through-plane (z-axis), included the GDE, stagnant boundary layers on both sides, and ideally mixed bulk phases. The model also employed a Leverett approach to capture gas-liquid coexistence in the porous GDE, incorporating electrowetting effects on silver's potential-dependent contact angle. Fitted to steady-state experimental data for sprayed electrodes with diluted CO_2 feeds, the model identified high electrolyte saturation as the primary cause of mass transfer limitations at high current densities. Additionally, potassium carbonate (K_2CO_3) precipitation due to local supersaturation was identified as a degradation mechanism above 300 mA cm^{-2}. Furthermore, their model suggested that more hydrophobic and thinner GDEs enhance performance.

As shown in Table 6, 2D modeling studies of electrochemical CO_2 reduction remain relatively scarce in the literature. Among the few, Kannan et al.[276] employed Monte Carlo simulations (MCS) using a 2D mechanistic model for the electrochemical conversion of CO_2 to CO in a microfluidic flow cell reactor. Both intrinsic material and electrochemical properties, as well as extrinsic operating conditions and design parameters, affected the performance, conversion efficiency, and selectivity. Parameters were ranked based on their impact, revealing that the charge-transfer coefficients for CO and H_2 formation and catalyst properties are the most influential ones across all potentials. Alongside this research, Kas et al.[275] presented a 2D transport model for a GDE performing CO_2 reduction to CO with a flowing catholyte. Specifically, the cathode compartment of a PEM-based CO_2 electrolyzer with a flowing catholyte configuration was modeled at steady state using a 2D finite element approach. The 2D model provided longitudinal insights into concentration gradients within the gas and electrolyte flow channels. It quantified concentration overpotentials and Ohmic drops across a range of potentials, exploring their impact on the CO_2 mass transfer-limited current density, conversion, and outlet gas composition. Understanding all these process interactions will aid in the design of more efficient electrolyzers.

Complementing this work, Löffelholz et al.[274] developed a spatially resolved pseudo-2D mathematical model for low-temperature eCO_2R at silver GDEs and validated it by studying flow cell experiments. The model, which included the GDE and two stagnant films (gas and electrolyte side), highlighted key limitations in eCO_2R efficiency: CO_2 mass transport constraints at high current densities and low carbon utilization efficiency due to chemical absorption of CO_2 in the electrolyte. It accurately predicted the overpotential and the Faradaic efficiency across varying $KHCO_3$ concentrations and CO_2 feed fractions.

While the previously discussed studies primarily focused on GDE-type cell configurations, as illustrated in Figure 3, there are comparatively fewer modeling efforts addressing alternative cell configurations. Notably, Weng et al.[277] presented a modeling framework for an AEM-MEA cell performing eCO_2R with a silver catalyst with either pure gaseous feeds (full-MEA) or a gaseous cathode feed and aqueous anode feed (exchange-MEA). The model accounted for mass transport, electrochemical and homogeneous reaction kinetics, and thermal effects. Simulation results were used to evaluate different MEA designs, highlighting their advantages, limitations, and strategies for improving water management and overall efficiency. Extending this line of investigation, Lees et al.[273] employed multi-physics modeling to analyze the CO_2 reduction to CO in a membrane-electrode-assembly setup with silver catalysts. They implemented a 1D model to simulate the partial current densities for H_2, CO, and O_2 formation within a CO_2 electrolyzer MEA, along with carbon crossover from the cathode to the anode, providing insights into optimizing the CO_2 electrolyzer performance. Their study highlighted key performance factors, such as ion transport, CO_2 solubility, and water management. Their simulations indicated that enhancing the ion-exchange capacity and catalyst surface area could improve CO formation rates without compromising CO_2 utilization.

Lastly, Bui et al.[278] conducted a comprehensive review on eCO_2R, positioning it as an ideal model reaction for studying electrochemical synthesis in porous electrodes due to its diverse product distribution and strong sensitivity to the local chemical environment. They emphasized that the transport of gases, liquids, and ions determines this chemical environment and consequently influences the electrochemical synthesis performance. Understanding how to control this environment was identified as crucial for enhancing the catalytic activity. However, they noted the difficulty in experimentally quantifying the concurrent rates of mass transfer and (electro)chemical reactions due to their occurrence across various length and time scales. To address this, their review highlighted how modeling had been used to correlate the dynamic chemical environment within porous electrodes with experimentally observable variables and values, such as the product distribution, total current density, and thermodynamic efficiency. Importantly, these models aim not only to facilitate the design of porous electrodes from first principles but also to provide fundamental insights by identifying the roles of transport and reaction processes that remain inaccessible through current experimental methods.

While the previously described models provide mechanistic insights into the underlying species transport and cell performance, they are computationally expensive and time-consuming.[279] The challenge in employing these models becomes apparent when one must perform multivariate optimization or uncertainty analysis. Numerical models must be run multiple times to perform optimization, which becomes a significant bottleneck owing to their high computational cost, making them less efficient for parameter optimization and real-time analysis. Data-driven models have emerged as a promising cost-effective approach to perform multi-variable optimization[280] and sensitivity analysis.[281] These methods use statistical algorithms, which learn the relationship between input parameters and output variables from numerical or experimental data.[282] Considerable amounts of work on deploying data-driven models for optimization and real-time analysis of proton exchange membrane fuel cells (PEMFC) exist both at the cell level and for fuel cell stacks.[283] However, there is a scarcity in the literature on the usage of data-driven models for CO_2 electrochemical conversion at the cell and stack level.

Grega et al.[284] used experimental data obtained from an automated platform (AdaCarbon), which fabricates and characterizes GDE for CO_2 electrolysis, to develop a hybrid ML-based continuum model. They used a multilayer perceptron architecture to map five experimental input parameters (Nafion volume, composition ratio of Ag:Cu, Sustainion volume, catalyst mass loading, and mass-averaged catalyst density) to six pre-sample inputs, which were provided as modeling parameters for a

physics-based continuum model.[272] This hybrid model allowed capturing multi-product reactions with CO and ethylene as products. Furthermore, the authors augmented a Gaussian process with the hybrid model to perform uncertainty analysis. The extended adaptive hybrid function (E-AHF) approach was used to perform multi-variable multi-objective optimization of a GDE-based eCO_2R system.[285] The E-AHF methodology is an ensemble of five different surrogate models, namely support vector regression (SVR), kriging, polynomial response surface, radial basis function, and moving least squares. Predictions from the model were made as a weighted summation of predictions made by individual surrogate models. An experimentally validated 2D, multi-physics, multiphase, isothermal model of a GDE-based microfluidic cell was used to generate the dataset to train the E-AHF surrogate model. The authors selected three electrode parameters and five operating conditions as input parameters to map the product yield, CO_2 conversion rate, and specific electrical energy consumption (SEEC) of the eCO_2R cell. Sobol's global sensitivity analysis[286] was performed using a variance-based Monte Carlo method, indicating that product yield and conversion rate were most sensitive to the electrolyte concentration, whereas the cathode potential impacted the SEEC the most. Furthermore, optimization performed using the surrogate model improved the performance of the electrochemical reactor by providing optimal parameters, which reduced the SEEC by ≈50% and increased the product yield and conversion rate by two times. A similar approach was undertaken by Tai et al.[280] in which they used deep neural networks to develop a data-driven model from data generated from a physics-based 2D model. However, their framework also included the use of a bi-directional long short-term memory (LSTM) model to forecast meteorological data from renewably generated electricity, which in turn, provided a dynamic supply of input current density to the electrolyzer stack.

The advantage of data-driven models is evident when performing scale-up studies for CO_2 electrolysis. Using a hybrid data-driven and 2D continuum model for eCO_2R, Zhang et al.[287] systematically investigated the consumption of CO_2 within the catalyst layer when the electrode area is scaled up from 1 to 100 cm^2. They selected four key variables, namely, electrode area (1–100 cm^2), catalyst layer thickness (1–100 µm), gas flow rate (1–100 mL min^{-1}), and GDL porosity (0.5–0.9), wherein each variable had six levels. Latin hypercube sampling was used as a sampling technique to extract data points at different levels while ensuring a uniform positional distribution.[288] The researchers compared the performance of SVR, random forest (RF), and recurrent neural network (RNN) algorithms trained on the sampled dataset. Using the hybrid modeling approach, the authors achieved a maximum CO_2 consumption rate of 98% at an electrode area of 100 cm^2, which was sustained throughout the scale-up process. Furthermore, the feature importance analysis with RF identified the catalyst layer thickness, electrode area, and gas flow rate as the key parameters.

Data-driven models are often black-box in nature and suffer from a lack of interpretability. Recent advances in this direction have been made under the domain of explainable artificial intelligence (XAI) to alleviate this problem. XAI techniques like SHapley Additive exPlanations and local interpretable model-agnostic explanations can be useful in screening key experimental parameters, which strongly influence the experimental performance metrics like CO Faradaic efficiency and selectivity. Combined with high-throughput experimentation (HTE), this approach accelerates parameter screening and guides design choices for scaling from lab to industry. HTE builds on parallelization, automation, modularization, and standardization, requiring automated experimental design and data analysis for a streamlined workflow.[289] Real-time analysis can be enabled by ML and XAI, which operate on high-dimensional, correlated parameter spaces (process, electrochemical, and component parameters). However, even with HTE, data may remain insufficient, making hybrid models a necessary first step.

Currently, performance data are largely limited to small lab-scale cells (≈5 cm^2), far below industrial-scale requirements (≈1 m^2). To address this gap, Blake et al. developed a 2D model comparing lab- and large-scale electrolyzers, revealing that larger systems experience greater inhomogeneities, elevated pH, thicker boundary layers, higher overpotentials, and increased CO_2 losses.[290] Similarly, Bahreini et al. validated a 2D transient-state model for formate production, showing that scaling induces pronounced pH gradients, CO_2 depletion, and localized efficiency losses, which represent major barriers to uniform performance.[291] Therefore, model validation for industrially relevant cells should be focused on spatial inhomogeneities (e.g., across electrodes) and be benchmarked against experimentally measured profiles. For example, single cells should be equipped with (arrays of) sensors to monitor the local values of parameters, such as temperature, pressure, and potential. To strengthen comparability and validity, harmonized models, experimental protocols, and cell configurations, also within the framework of inter-laboratory studies, would be desirable. Finally, the use of data-driven models for real-time monitoring and control is well established in PEM fuel cells/stacks.[292] Time series forecasting methods like RNN and LSTM have been deployed to perform predictive control of the electrochemical system by anticipating undesired changes.[293] With the aid of the predictions made by these models, one can deploy adaptive control strategies to be able to foresee early indicators of system failure.[294,295] Adapting these approaches, which are capable of real-time monitoring and optimization, is essential for scaling up CO_2 electrolysis toward the industrial scale.

6. Conclusion and Perspective

In this work, the published research activities from the past ten years on the development of Ag-based GDEs for the application of electrochemical CO_2 to CO conversion were analyzed. The respective electrode designs and experimental laboratory cell configurations were compared, as well as the employed electrode fabrication methods. In the academic landscape, carbon-based GDEs far outnumber any other variants. The most prominent non-carbon-based GDEs are PTFE-based when considering studies beyond the laboratory scale of ≈10 cm^2. The highest reported current densities were on the order of 1–4 A cm^{-2}, well within the domain known from water electrolysis, thus demonstrating the potential for real-world implementation. To date, the largest Ag-based electrode area reported is 300 cm^2, featuring a Faradaic efficiency of 95%. This geometric scale was also extended to a stack consisting of ten such cells. Further, long-duration tests were performed for ≈4000 h with a single cell, albeit still with a

small active cell area of 5 cm^2. In addition, and in complementary ways, physics-based and data-driven models driven by machine learning will greatly accelerate further development with respect to Ag-GDE design and operation.

For future experimental work and modeling efforts, we recommend the following:

1) A more rigorous approach in terms of reporting all relevant information, especially with respect to the catalyst and ionomer loading and the description of the electrode fabrication steps, is required. It is also crucial to specify all parameters employed for testing with half-cell and full-cell setups. The composition of the catalyst layer should also be investigated in more detail, namely with pristine samples and post-test and post-mortem, implementing microscopic analyses, spectroscopy, and X-ray techniques. To refine techno-economic and life cycle assessments, a focus on revealing and mitigating degradation phenomena and lifetime prediction based on accelerated stress tests should be implemented.
2) With respect to scaling catalyst production, one should be mindful that, although silver is currently significantly less expensive than noble metals, future market volatilities cannot be ruled out entirely, especially considering the accelerating expansion of photovoltaics. Therefore, minimizing the catalyst loading and reducing excess waste in the fabrication process is critical, as well as developing economically viable recycling routes. Moreover, research on silver alternatives should be continued, with a focus on scaling up the synthesis procedures. Due to potentially more stringent environmental regulations in the coming years, it is pertinent to develop and incorporate alternative binders and ionomers that do not contain perfluorosulfonic acid compounds.
3) Physics-based modeling of eCO_2R has gained momentum in recent years, yet it remains relatively underdeveloped compared to models describing more mature electrochemical systems like PEM water electrolyzers. While some studies have incorporated microkinetic insights or techno-economic considerations, comprehensive multi-scale models, transient simulations, and detailed parametric studies are still scarce. In this context, Yanzheng He et al. emphasized the importance of coupling density functional theory (DFT), molecular dynamics (MD), and FEM to address the full complexity of eCO_2R, bridging atomic-level mechanisms with macroscopic behavior.[296] In a more recent work, the same authors further highlighted that integrating multiscale simulations with real-world parameters, such as pH, solvent effects, and applied potential, will be key to developing predictive, high-fidelity models capable of guiding the rational design of next-generation CO_2 electrolyzers.[297]
4) The development of data-driven models for the electrochemical reduction of CO_2 to CO is still in its early stages. While considerable efforts have been made in using machine learning to screen electrocatalysts for CO_2 reduction, the lack of similar progress in data-driven modeling at a macroscopic cell/component level has so far been a missed opportunity to further drive efficiency to optimize and scale up. There are a few works that combine physics-based 1D/2D models with machine learning to perform sensitivity analyses and multi-objective optimization. Therefore, further exploration into developing these hybrid physics-based AI models must be undertaken with higher-dimensional numerical models at the cell and stack levels. Moreover, since the electrochemical reduction of CO_2 is a complex process, which is dependent on several parameters and is hampered by side reactions, it is pertinent to use experimental data to develop accurate data-driven models, which can simultaneously capture degradation and electrode flooding in real-time, as well as variability due to fabrication methods. Accounting for all these factors through numerical simulations is a challenging task, and experimental data captures these effects implicitly. Therefore, experimental-based data-driven models can provide a higher degree of insight for the optimization and scale-up in industrial application scenarios.
5) With respect to viable continuous GDE fabrication processes, most likely spray coating or slot die coating would be the methods of choice for industrial manufacturing, provided the catalyst ink is sufficiently stable, offers adequate viscosity behavior, and the required drying period is compatible with the other process parameters. Apparatuses that monitor the fabrication steps are required to ensure consistent quality with minimal tolerances regarding key parameters, such as the ionomer or binder content and catalyst loading. Ideally, such devices would be incorporated directly into the manufacturing line, acquiring data in real time to enable immediate action, should the required specifications not be met, such as, e.g., the appropriate electrode coating thickness. Inks, slurries, or pastes should be characterized rheologically immediately before the coating process, ideally in an automated manner. The thickness and homogeneity of coatings should be monitored continuously. The interfaces within the GDE must be tailored for optimal functionality of the catalyst, but also all interfaces in the cell as well, to ensure optimal electrical contact, potential distribution, and mass transport. Interfacial design considerations, therefore, affect electrode performance and are crucial in assessing the scalability of electrode concepts from laboratory studies to industrial implementation. With respect to future work, it may be worthwhile to study novel electrode architectures that feature gradients across the electrode thickness with respect to the catalyst and ionomer content, as well as the pore size, to further optimize performance while trying to minimize the catalyst and ionomer loading.
6) With respect to cell operation, a major challenge lies in maintaining the proper degree of humidification, respectively wetting of the electrode surface, and the optimal pressure differential under varying current load, as would be the case if the cell or stack were directly coupled with an intermittent power source. Further, the hydrostatic pressure in the electrolyte gap depends on the height of the electrode. At a certain height, this affects the flooding behavior of the cathode, which would require engineering design measures to adapt the flow configuration within the cell, should the objective be to greatly increase the geometric area as opposed to cell stacking.[79,81] In addition, current-dependent electrowetting is an important phenomenon that affects flooding as well. Care must also be taken during operation in the field to avoid degradation of the electrodes. For instance, during standby, the cell should be held at a discrete constant potential so that

a deteriorating reversal of the cell potential is prevented at all times.[298] Otherwise, the silver catalyst may be oxidized irreversibly, thus greatly decreasing the electrochemical activity of the cathode. Further, intermittent operation following a virtual power output profile as it would be provided by a photovoltaic plant, revealed that while overall operation over 500 h was demonstrated, distinct spikes with very high rates of hydrogen evolution were also observed.[299] In light of these intricacies, it is pertinent to design algorithms for cell operation that account for dynamic changes with respect to the above-mentioned parameters to ensure optimal cell operation with rapid response times, especially when coupling CO_2 electrolyzers directly with intermittent sources of renewably generated electricity.

7) Statistical experimental design, e.g., with factorial experiments, may be employed to evaluate the impact and interaction of the key operating parameters with the Faradaic efficiency or cell voltage employed as response variables, thus ideally allowing more rapid optimization. Based on promising results obtained with simulations by Zhang et al., it can be hypothesized that the application of design of experiment-based methods could also lead to an in-depth understanding and optimization in experimental work.[287]
8) Combined with advanced modeling and optimization of the balance of plant in the context of stacking cells of appropriate active area, the abovementioned approaches will enable the deployment of CO_2 electrolyzers as either stand-alone devices or as integrated units within major chemical plants, provided economic criteria will be met as well.

Supporting Information

Supporting Information is available from the Wiley Online Library or from the author.

Acknowledgements

The authors thank the German Federal Ministry of Research, Technology, and Space, BMFTR, for the funding received within the project Power2ValueChemicals (Grant No. 03SFK2S5C). S.E. would like to express his deepest appreciation to Darius Gahr for his dedicated support with the laboratory work.

Open access funding enabled and organized by Projekt DEAL.

Conflict of Interest

The authors declare no conflict of interest.

Keywords

CO_2 electrolysis, data-driven modeling, gas diffusion electrodes, numerical simulations, scale-up, silver electrocatalysts

Received: August 26, 2025
Revised: October 9, 2025
Published online:

[1] H. McLaughlin, A. A. Littlefield, M. Menefee, A. Kinzer, T. Hull, B. K. Sovacool, M. D. Bazilian, J. Kim, S. Griffiths, *Renew. Sustain. Energy Rev.* **2023**, *177*, 113215.
[2] W. K. Shi, Y. Ji, X. J. Zhang, M. X. Fang, T. Wang, L. Jiang, *Carbon Capture Sci. Technol.* **2023**, *7*, 100114.
[3] Y. Pei, H. Zhong, F. Jin, *Energy Sci. Eng.* **2021**, *9*, 1012.
[4] D. M. Weekes, D. A. Salvatore, A. Reyes, A. Huang, C. P. Berlinguette, *Acc. Chem. Res.* **2018**, *51*, 910.
[5] N. T. Nesbitt, T. Burdyny, H. Simonson, D. Salvatore, D. Bohra, R. Kas, W. A. Smith, *ACS Catal.* **2020**, *10*, 14093.
[6] Y. Wu, S. Garg, M. Li, M. N. Idros, Z. Li, R. Lin, J. Chen, G. Wang, T. E. Rufford, *J. Power Sources* **2022**, *522*, 230998.
[7] H. Lee, S. Kwon, N. Park, S. G. Cha, E. Lee, T.-H. Kong, J. Cha, Y. Kwon, *JACS Au* **2024**, *4*, 3383.
[8] J. Lin, S. Yan, C. Zhang, Q. Hu, Z. Cheng, *Processes* **2022**, *10*, 826.
[9] R. J. Detz, C. J. Ferchaud, A. J. Kalkman, J. Kemper, C. Sánchez-Martínez, M. Saric, M. V. Shinde, *Sustain. Energy Fuels* **2023**, *7*, 5445.
[10] A. Somoza-Tornos, O. J. Guerra, A. M. Crow, W. A. Smith, B.-M. Hodge, *iScience* **2021**, *24*, 102813.
[11] I. Bagemihl, L. Cammann, M. Pérez-Fortes, V. van Steijn, J. R. van Ommen, *ACS Sustainable Chem. Eng.* **2023**, *11*, 10130.
[12] D. Wakerley, S. Lamaison, J. Wicks, A. Clemens, J. Feaster, D. Corral, S A. Jaffer, A. Sarkar, M. Fontecave, E B. Duoss, S. Baker, E H. Sargent, T F. Jaramillo, C. Hahn, *Nat. Energy* **2022**, *7*, 130.
[13] Z. Liu, J. Qian, G. Zhang, B. Zhang, Y. He, *Sep. Purif. Technol.* **2024**, *330*, 125177.
[14] A. Liu, M. Gao, X. Ren, F. Meng, Y. Yang, L. Gao, Q. Yang, T. Ma, *J. Mater. Chem. A* **2020**, *8*, 3541.
[15] Y. Chen, S. Hu, X. Kang, B. Liu, *MRS Energy Sustain* **2025**, *12*, 121.
[16] J. Osiewacz, B. Ellendorff, U. Kunz, T. Turek, *J. Electrochem. Soc.* **2024**, *171*, 103503.
[17] X. She, T. Zhang, Z. Li, H. Li, H. Xu, J. Wu, *Cell Rep. Phys. Sci.* **2020**, *1*, 100051.
[18] C. Chen, Y. Li, S. Yu, S. Louisia, J. Jin, M. Li, M. B. Ross, P. Yang, *Joule* **2020**, *4*, 1688.
[19] N. Sikdar, J. R. C. Junqueira, D. Öhl, S. Dieckhöfer, T. Quast, M. Braun, H. B. Aiyappa, S. Seisel, C. Andronescu, W. Schuhmann, *Chem. - Eur. J.* **2022**, *28*, 202104249.
[20] J. Qin, T. Wang, M. Zhai, C. Wu, Y. A. Liu, B. Yang, H. Yang, K. Wen, W. Hu, *Adv. Funct. Mater.* **2023**, *33*, 2300697.
[21] W. Ni, H. Chen, N. Tang, T. Hu, W. Zhang, Y. Zhang, S. Zhang, *Nat. Commun.* **2024**, *15*, 6078.
[22] Y. Kong, H. Hu, M. Liu, Y. Hou, V. Kolivoška, S. Vesztergom, P. Broekmann, *J. Catal.* **2022**, *408*, 1.
[23] M. Li, M. N. Idros, Y. Wu, T. Burdyny, S. Garg, X. S. Zhao, G. Wang, T. E. Rufford, *J. Mater. Chem. A* **2021**, *9*, 19369.
[24] M. E. Leonard, L. E. Clarke, A. Forner-Cuenca, S. M. Brown, F. R. Brushett, *ChemSusChem* **2020**, *13*, 400.
[25] P. Jeanty, C. Scherer, E. Magori, K. Wiesner-Fleischer, O. Hinrichsen, M. Fleischer, *J. CO2 Util.* **2018**, *24*, 454.
[26] H. Hu, Y. Kong, M. Liu, V. Kolivoška, A. V. Rudnev, Y. Hou, R. Erni, S. Vesztergom, P. Broekmann, *J. Mater. Chem. A* **2023**, *11*, 5083.
[27] P. Gonugunta, K. Roohi, M. Soleimani, P. R. Anusuyadevi, P. Taheri, M. Ramdin, *Ind. Eng. Chem. Res.* **2025**, *64*, 2113.
[28] S. Hernandez-Aldave, E. Andreoli, *Catalysts* **2020**, *10*, 713.
[29] T. Burdyny, W. A. Smith, *Energy Environ. Sci.* **2019**, *12*, 1442.
[30] Y. Kuang, G. Chen, H. Rabiee, B. Ma, F. Dorosti, A. K. Nanjundan, Z. Zhu, H. Wang, L. Ge, *Energy Fuels* **2024**, *38*, 10096.
[31] F. Bienen, M. C. Paulisch, T. Mager, J. Osiewacz, M. Nazari, M. Osenberg, B. Ellendorff, T. Turek, U. Nieken, I. Manke, K. A. Friedrich, *Electrochem. Sci. Adv.* **2023**, *3*, 2100158.
[32] G. O. Larrazábal, P. Strøm-Hansen, J. P. Heli, K. Zeiter, K. T. Therkildsen, I. Chorkendorff, B. Seger, *ACS Appl. Mater. Interfaces* **2019**, *11*, 41281.
[33] C.-T. Dinh, F. P. García de Arquer, D. Sinton, E. H. Sargent, *ACS Energy Lett.* **2018**, *3*, 2835.

[34] C.-T. Dinh, T. Burdyny, Md G Kibria, A. Seifitokaldani, C M. Gabardo, F. P García de Arquer, A. Kiani, J P. Edwards, P. De Luna, O S. Bushuyev, C. Zou, R. Quintero-Bermudez, Y. Pang, D. Sinton, E H. Sargent, *Science* **2018**, *360*, 783.
[35] K. Qi, Y. Zhang, Ji Li, C. Charmette, M. Ramonda, X. Cui, Y. Wang, Y. Zhang, H. Wu, W. Wang, X. Zhang, D. Voiry, *ACS Nano* **2021**, *15*, 7682.
[36] E. B. Nursanto, H. Da Won, M. S. Jee, H. Kim, N.-K. Kim, K. D. Jung, Y. J. Hwang, B. K. Min, *Top. Catal.* **2018**, *61*, 389.
[37] S.-Q. Liu, S.-W. Wu, M.-R. Gao, M.-S. Li, X.-Z. Fu, J.-L. Luo, *ACS Sustainable Chem. Eng.* **2019**, *7*, 14443.
[38] C. Lee, B. Zhao, J. K. Lee, K. F. Fahy, K. Krause, A. Bazylak, *iScience* **2020**, *23*, 101094.
[39] B. Endrődi, E. Kecsenovity, A. Samu, T. Halmágyi, S. Rojas-Carbonell, L. Wang, Y. Yan, C. Janáky, *Energy Environ. Sci.* **2020**, *13*, 4098.
[40] B. Endrődi, E. Kecsenovity, A. Samu, F. Darvas, R. V. Jones, V. Török, A. Danyi, C. Janáky, *ACS Energy Lett.* **2019**, *4*, 1770.
[41] R. Krause, D. Reinisch, C. Reller, H. Eckert, D. Hartmann, D. Taroata, K. Wiesner-Fleischer, A. Bulan, A. Lueken, G. Schmid, *Chem. Ing. Tech.* **2020**, *92*, 53.
[42] J. A. Rabinowitz, M. W. Kanan, *Nat. Commun.* **2020**, *11*, 5231.
[43] A. Ozden, F. P García de Arquer, J. E. Huang, J. Wicks, J. Sisler, R. K. Miao, C. P. O'Brien, G. Lee, X. Wang, A. H. Ip, E. H. Sargent, D. Sinton, *Nat. Sustain.* **2022**, *5*, 563.
[44] M. Ma, E. L. Clark, K. T. Therkildsen, S. Dalsgaard, I. Chorkendorff, B. Seger, *Energy Environ. Sci.* **2020**, *13*, 977.
[45] A. Wang, W. Ge, W. Sun, X. Sheng, L. Dong, W. Zhang, H. Jiang, C. Li, *Angew. Chem., Int. Ed.* **2025**, *64*, 202412754.
[46] W. Ge, L. Dong, C. Wang, Y. Zhu, Z. Liu, H. Jiang, C. Li, *ACS Catal.* **2024**, *14*, 10529.
[47] S. Alinejad, J. Quinson, Y. Li, Y. Kong, S. Reichenberger, S. Barcikowski, P. Broekmann, M. Arenz, *J. Catal.* **2024**, *429*, 115209.
[48] M. Liu, H. Hu, Y. Kong, I. Z. Montiel, V. Kolivoška, A. V. Rudnev, Y. Hou, R. Erni, S. Vesztergom, P. Broekmann, *Appl. Catal. B* **2023**, *335*, 122885.
[49] H. Hu, M. Liu, Y. Kong, I. Z. Montiel, Y. Hou, A. V. Rudnev, P. Broekmann, *ChemElectroChem* **2022**, *9*, 202200615.
[50] R. Wang, H. Haspel, A. Pustovarenko, A. Dikhtiarenko, A. Russkikh, G. Shterk, D. Osadchii, S. Ould-Chikh, M. Ma, W. A. Smith, K. Takanabe, *ACS Energy Lett.* **2019**, *4*, 2024.
[51] P. Karimi, A. Alihosseinzadeh, S. Ponnurangam, K. Karan, *J. Electrochem. Soc.* **2022**, *169*, 064510.
[52] D. G. Wheeler, B. A. W. Mowbray, A. Reyes, F. Habibzadeh, J. He, C. P. Berlinguette, *Energy Environ. Sci.* **2020**, *13*, 5126.
[53] R. P. Morco, L. A. Diaz, M. M. Ramirez-Corredores, *Sustain. Energy Fuels* **2025**, *9*, 424.
[54] X. Du, P. Zhang, G. Zhang, H. Gao, L. Zhang, M. Zhang, T. Wang, J. Gong, *Natl. Sci. Rev.* **2024**, *11*, nwad149.
[55] C. Martens, B. Schmid, H. Tempel, R.-A. Eichel, *Green Chem.* **2023**, *25*, 7794.
[56] S. Verma, X. Lu, S. Ma, R. I. Masel, P. J. A. Kenis, *Phys. Chem. Chem. Phys.* **2016**, *18*, 7075.
[57] B. Kim, S. Ma, H.-R. M Jhong, P. J. Kenis, *Electrochim. Acta* **2015**, *166*, 271.
[58] S. Wu, Y. Hua, J. Zhang, F. Shen, W. Song, X. Zhang, J. Liu, B. Yang, Y. Dai, J. Shi, *Energy Fuels* **2022**, *36*, 3771.
[59] S. Li, X. Dong, W. Chen, Y. Song, G. Li, W. Wei, Y. Sun, *Catalysts* **2022**, *12*, 453.
[60] F. Mattarozzi, N. van der Willige, V. Gulino, C. Keijzer, R. C. J. van de Poll, E. J. M. Hensen, P. Ngene, P. E. de Jongh, *ChemCatChem* **2023**, *15*, 202300792.
[61] A. Seifitokaldani, C. M. Gabardo, T. Burdyny, C.-T. Dinh, J. P. Edwards, M. G. Kibria, O. S. Bushuyev, S. O. Kelley, D. Sinton, E. H. Sargent, *J. Am. Chem. Soc.* **2018**, *140*, 3833.
[62] W. H. Lee, Y.-J. Ko, Y. Choi, S. Y. Lee, C. H. Choi, Y. J. Hwang, B. K. Min, P. Strasser, H.-S. Oh, *Nano Energy* **2020**, *76*, 105030.
[63] X. Deng, D. Alfonso, T.-D. Nguyen-Phan, D. R. Kauffman, *ACS Catal.* **2022**, *12*, 5921.
[64] Z. Min, B. Chang, C. Shao, X. Su, N. Wang, Z. Li, H. Wang, Y. Zhao, M. Fan, J. Wang, *Appl. Catal. B* **2023**, *326*, 122185.
[65] H. Tao, H. Chang, F. Wang, Z. Zhang, S. Min, *Sustain. Energy Fuels* **2024**, *8*, 1641.
[66] Y. Kim, E. W. Lees, C. P. Berlinguette, *ACS Energy Lett.* **2022**, *7*, 2382.
[67] Z. He, T. Liu, J. Tang, C. Zhou, L. Wen, J. Chen, S. Song, *Electrochim. Acta* **2016**, *222*, 1234.
[68] Y. S. Ham, S. Choe, M. J. Kim, T. Lim, S.-K. Kim, J. J. Kim, *Appl. Catal. B* **2017**, *208*, 35.
[69] M. Ma, B. J. Trześniewski, J. Xie, W. A. Smith, *Angew. Chem., Int. Ed.* **2016**, *55*, 9748.
[70] M. S. Jee, H. Kim, H. S. Jeon, K. H. Chae, J. Cho, B. K. Min, Y. J. Hwang, *Catal. Today* **2017**, *288*, 48.
[71] Y.-C. Hsieh, L. E. Betancourt, S. D. Senanayake, E. Hu, Y. Zhang, W. Xu, D. E. Polyansky, *ACS Appl. Energy Mater.* **2019**, *2*, 102.
[72] W. Luc, J. Rosen, F. Jiao, *Catal. Today* **2017**, *288*, 79.
[73] J. Rosen, G. S. Hutchings, Q. Lu, S. Rivera, Y. Zhou, D. G. Vlachos, F. Jiao, *ACS Catal.* **2015**, *5*, 4293.
[74] T. Haas, R. Krause, R. Weber, M. Demler, G. Schmid, *Nat. Catal.* **2018**, *1*, 32.
[75] M. Quentmeier, B. Schmid, H. Tempel, H. Kungl, R.-A. Eichel, *ACS Sustainable Chem. Eng.* **2023**, *11*, 679.
[76] B. Kim, F. Hillman, M. Ariyoshi, S. Fujikawa, P. J. Kenis, *J. Power Sources* **2016**, *312*, 192.
[77] S. Ma, R. Luo, J. I. Gold, A. Z. Yu, B. Kim, P. J. A. Kenis, *J. Mater. Chem. A* **2016**, *4*, 8573.
[78] E. R. Cofell, U. O. Nwabara, S. S. Bhargava, D. E. Henckel, P. J. A. Kenis, *ACS Appl. Mater. Interfaces* **2021**, *13*, 15132.
[79] L. M. Baumgartner, C. I. Koopman, A. Forner-Cuenca, D. A. Vermaas, *ACS Appl. Energy Mater.* **2022**, *5*, 15125.
[80] S. S. Bhargava, D. Azmoodeh, X. Chen, E. R. Cofell, A. M. Esposito, S. Verma, A. A. Gewirth, P. J. A. Kenis, *ACS Energy Lett.* **2021**, *6*, 2427.
[81] L. M. Baumgartner, C. I. Koopman, A. Forner-Cuenca, D. A. Vermaas, *ACS Sustainable Chem. Eng.* **2022**, *10*, 4683.
[82] K. Krause, C. Lee, J. K. Lee, K. F. Fahy, H. W. Shafaque, P. J. Kim, P. Shrestha, A. Bazylak, *ACS Sustainable Chem. Eng.* **2021**, *9*, 5570.
[83] U. O. Nwabara, A. D. Hernandez, D. A. Henckel, X. Chen, E. R. Cofell, M. P. de-Heer, S. Verma, A. A. Gewirth, P. J. A. Kenis, *ACS Appl. Energy Mater.* **2021**, *4*, 5175.
[84] K. Seteiz, J. N. Häberlein, P. A. Heizmann, J. Disch, S. Vierrath, *RSC Adv.* **2023**, *13*, 18916.
[85] V. Chanda, D. Blaudszun, L. Hoof, I. Sanjuán, K. Pellumbi, K. junge Puring, C. Andronescu, U.-P. Apfel, *ChemElectroChem* **2024**, *11*, 202300715.
[86] E. W. Lees, B. A. W. Mowbray, D. A. Salvatore, G. L. Simpson, D. J. Dvorak, S. Ren, J. Chau, K. L. Milton, C. P. Berlinguette, *J. Mater. Chem. A* **2020**, *8*, 19493.
[87] M. Bühler, F. Hegge, P. Holzapfel, M. Bierling, M. Suermann, S. Vierrath, S. Thiele, *J. Mater. Chem. A* **2019**, *7*, 26984.
[88] B. Mayerhöfer, K. Ehelebe, F. D. Speck, M. Bierling, J. Bender, J. A. Kerres, K. J. J. Mayrhofer, S. Cherevko, R. Peach, S. Thiele, *J. Mater. Chem. A* **2021**, *9*, 14285.
[89] B. Mayerhöfer, D. McLaughlin, T. Böhm, M. Hegelheimer, D. Seeberger, S. Thiele, *ACS Appl. Energy Mater.* **2020**, *3*, 9635.
[90] L. M. Baumgartner, A. Goryachev, C. I. Koopman, D. Franzen, B. Ellendorff, T. Turek, D. A. Vermaas, *Energy Adv* **2023**, *2*, 1893.
[91] H. Deng, Z. Chen, Y. Wang, *ChemSusChem* **2025**, *18*, 202401728.

[92] T. Möller, T. Ngo Thanh, X. Wang, W. Ju, Z. Jovanov, P. Strasser, *Energy Environ. Sci.* **2021**, *14*, 5995.
[93] R. B. Kutz, Q. Chen, H. Yang, S. D. Sajjad, Z. Liu, I. R. Masel, *Energy Technol.* **2017**, *5*, 929.
[94] Z. Liu, H. Yang, R. Kutz, R. I. Masel, *J. Electrochem. Soc.* **2018**, *165*, J3371.
[95] J. Fan, B. Pan, J. Wu, C. Shao, Z. Wen, Y. Yan, Y. Wang, Y. Li, *Angew. Chem., Int. Ed.* **2024**, *63*, 202317828.
[96] S. Zhang, Z. Mo, J. Wang, H. Liu, P. Liu, D. Hu, T. Tan, C. Wang, *Electrochim. Acta* **2021**, *390*, 138831.
[97] J. Chen, X. Liu, S. Xi, T. Zhang, Z. Liu, J. Chen, L. Shen, S. Kawi, L. Wang, *ACS Nano* **2022**, *16*, 13982.
[98] M. de Jesus Gálvez-Vázquez, P. Moreno-García, H. Xu, Y. Hou, H. Hu, I. Z. Montiel, A V. Rudnev, S. Alinejad, V. Grozovski, B J. Wiley, M. Arenz, P. Broekmann, *ACS Catal.* **2020**, *10*, 13096.
[99] M. Zhang, J. Zhao, S. Wei, *Energy Fuels* **2025**, *39*, 3169.
[100] D. A. Salvatore, D. M. Weekes, J. He, K. E. Dettelbach, Y. C. Li, T. E. Mallouk, C. P. Berlinguette, *ACS Energy Lett.* **2018**, *3*, 149.
[101] I. Moussallem, S. Pinnow, N. Wagner, T. Turek, *Chem. Eng. Process.: Process Intensif.* **2012**, *52*, 125.
[102] J. Osiewacz, M. Löffelholz, B. Ellendorff, T. Turek, *J. Power Sources* **2024**, *603*, 234430.
[103] H. Hoffmann, M. C. Paulisch, M. Gebhard, J. Osiewacz, M. Kutter, A. Hilger, T. Arlt, N. Kardjilov, B. Ellendorff, F. Beckmann, H. Markötter, M. Luik, T. Turek, I. Manke, C. Roth, *J. Electrochem. Soc.* **2022**, *169*, 044508.
[104] S. Magdassi, A. Bassa, Y. Vinetsky, A. Kamyshny, *Chem. Mater.* **2003**, *15*, 2208.
[105] S. Zhang, Y. Li, N. Pan, *J. Power Sources* **2012**, *206*, 476.
[106] J. H. Lee, B.-S. Kong, Y.-K. Baek, S. B. Yang, H.-T. Jung, *Nanotechnology* **2009**, *20*, 235203.
[107] V. Yarlagadda, S. E. McKinney, C. L. Keary, L. Thompson, B. Zulevi, A. Kongkanand, *J. Electrochem. Soc.* **2017**, *164*, F845.
[108] T. Kuang, J. Huang, J. Li, P. Yang, L. Zhang, D. Ye, X. Zhu, Q. Liao, *J. Power Sources* **2024**, *606*, 234543.
[109] W. Marchal, G. Vandevenne, J. D'Haen, A. Calmont de Andrade Almeida, M. A. Durand Sola, E. J. van den Ham, J. Drijkoningen, K. Elen, W. Deferme, M. K. Van Bael, A. Hardy, *Nanotechnology* **2017**, *28*, 215202.
[110] H. Shin, K. U. Hansen, F. Jiao, *Nat. Sustain.* **2021**, *4*, 911.
[111] M. G. Kibria, J. P. Edwards, C. M. Gabardo, C.-T. Dinh, A. Seifitokaldani, D. Sinton, E. H. Sargent, *Adv. Mater.* **2019**, *31*, 1807166.
[112] M. J. Orella, S. M. Brown, M. E. Leonard, Y. Román-Leshkov, F. R. Brushett, *Energy Technol.* **2020**, *8*, 1900994.
[113] C. Sauter, M. A. Emin, H. P. Schuchmann, S. Tavman, *Ultrason. Sonochem.* **2008**, *15*, 517.
[114] C.-N. Chen, Y.-L. Chen, W. J. Tseng, *J. Mater. Process. Technol.* **2007**, *190*, 61.
[115] S. Nitopi, E. Bertheussen, S B. Scott, X. Liu, A K. Engstfeld, S. Horch, B. Seger, I E. L. Stephens, K. Chan, C. Hahn, J K. Nørskov, T F. Jaramillo, Ib Chorkendorff, *Chem. Rev.* **2019**, *119*, 7610.
[116] J. Lin, Y. Zhang, P. Xu, L. Chen, *Mater. Rep. Energy* **2023**, *3*, 100194.
[117] D. S. Tran, N.-N. Vu, H.-E. Nemamcha, C. Boisvert, U. Legrand, A. G. Fink, F. Navarro-Pardo, C.-T. Dinh, P. Nguyen-Tri, *Coord. Chem. Rev.* **2025**, *524*, 216322.
[118] D. Song, S. Zhang, M. Zhou, M. Wang, R. Zhu, H. Ning, M. Wu, *ChemSusChem* **2024**, *17*, 202301719.
[119] S. A. Al-Tamreh, M. H. Ibrahim, M. H. El-Naas, J. Vaes, D. Pant, A. Benamor, A. Amhamed, *ChemElectroChem* **2021**, *8*, 3207.
[120] C. Minke, M. Suermann, B. Bensmann, R. Hanke-Rauschenbach, *Int. J. Hydrogen Energy* **2021**, *46*, 23581.
[121] A. A. Yaroshevsky, *Geochem. Int.* **2006**, *44*, 48.
[122] U. S. Geological Survey, "Mineral commodity summaries 2025", https://doi.org/10.3133/mcs2025 (accessed: September 2025).
[123] UNEP, "Recycling rates of metals-A status report", https://www.unep.org/resources/report/recycling-rates-metals-status-report (accessed: November 2025).
[124] Business Insider, "Commodities", https://markets.businessinsider.com/commodities (accessed: September 2025).
[125] B. Wire, "Ethylene Global Industry Report", https://www.businesswire.com/news/home/20240513898212/en/Ethylene-Global-Industry-Report-2024-2030-US-to-Dominate-Polyethylene-to-Account-for-Highest-Growth-Segment-ResearchAndMarkets.com (accessed: September 2025).
[126] ChemAnalyst, "Formic Acid Market", https://www.chemanalyst.com/industry-report/formic-acid-market-688 (accessed: September 2025).
[127] ChemAnalyst, "Methanol Market", https://www.chemanalyst.com/industry-report/methanol-market-219 (accessed: September 2025).
[128] The Silver Institute, "World Silver Survey 2025", https://silverinstitute.org/wp-content/uploads/2025/04/World_Silver_Survey-2025.pdf (accessed: September 2025).
[129] W. Li, T. Adachi, *Nat. Resour. Model.* **2019**, *32*, 12176.
[130] B. Hallam, M. Kim, Y. Zhang, L. Wang, A. Lennon, P. Verlinden, P. P. Altermatt, P. R. Dias, *Prog. Photovoltaics Res. Appl.* **2023**, *31*, 598.
[131] S. Lo Piano, A. Saltelli, J. P. van der Sluijs, *Front. Energy Res.* **2019**, *7*, 56.
[132] R. Paul, L. Zhu, H. Chen, J. Qu, L. Dai, *Adv. Mater.* **2019**, *31*, 1806403.
[133] X. Duan, J. Xu, Z. Wei, J. Ma, S. Guo, S. Wang, H. Liu, S. Dou, *Adv. Mater.* **2017**, *29*, 1701784.
[134] F. Franco, C. Rettenmaier, H. S. Jeon, B. R Cuenya, *Chem. Soc. Rev.* **2020**, *49*, 6884.
[135] M. Li, H. Wang, W. Luo, P. C. Sherrell, J. Chen, J. Yang, *Adv. Mater.* **2020**, *32*, 2001848.
[136] J. Liu, Y. Cai, R. Song, S. Ding, Z. Lyu, Y.-C. Chang, H. Tian, X. Zhang, D. Du, W. Zhu, Y. Zhou, Y. Lin, *Mater. Today* **2021**, *48*, 95.
[137] X. Xu, J. Guan, *Mater. Sci. Eng.: R: Rep.* **2025**, *162*, 100886.
[138] L. Qi, J. Guan, *Adv. Funct. Mater.* **2025**, *35*, 2500873.
[139] M. Chen, J. Guan, *Adv. Funct. Mater.* **2025**, *35*, 2423552.
[140] L. Qi, J. Guan, *Mater. Sci. Eng.: R: Rep.* **2025**, *166*, 101090.
[141] F. Yang, H. Yu, X. Mao, Q. Meng, S. Chen, Q. Deng, Z. Zeng, J. Wang, S. Deng, *Chem. Eng. J.* **2021**, *425*, 131661.
[142] H. Yang, Q. Lin, C. Zhang, X. Yu, Z. Cheng, G. Li, Qi Hu, X. Ren, Q. Zhang, J. Liu, C. He, *Nat. Commun.* **2020**, *11*, 593.
[143] X. Xu, J. Guan, *Adv. Funct. Mater.* **2025**, *35*, 2505823.
[144] J. Guo, H. Liu, D. Li, J. Wang, X. Djitcheu, D. He, Q. Zhang, *RSC Adv.* **2022**, *12*, 9373.
[145] M. Staudacher, D. Goes, S. Ahn, D. Vrucak, T. Gießmann, B. Bauer-Siebenlist, T. Leißner, M. Rudolph, J. Fleischer, B. Friedrich, U A. Peuker, *Recycling* **2025**, *10*, 121.
[146] M. Carmo, G. P. Keeley, D. Holtz, T. Grube, M. Robinius, M. Müller, D. Stolten, *Int. J. Hydrogen Energy* **2019**, *44*, 3450.
[147] A. Zupanc, J. Install, T. Weckman, M. M. Melander, M. Kemell, K. Honkala, T. Repo, *Chem. Eng. J.* **2025**, *512*, 162129.
[148] Y.-C. Hsieh, S. D. Senanayake, Y. Zhang, W. Xu, D. E. Polyansky, *ACS Catal.* **2015**, *5*, 5349.
[149] K. Sun, L. Wu, W. Qin, J. Zhou, Y. Hu, Z. Jiang, B. Shen, Z. Wang, *J. Mater. Chem. A* **2016**, *4*, 12616.
[150] H. Lee, S. H. Ahn, *Bull. Korean Chem. Soc.* **2017**, *38*, 1085.
[151] Q. Xu, A. Xu, S. Garg, A. B. Moss, I. Chorkendorff, T. Bligaard, B. Seger, *Angew. Chem., Int. Ed.* **2023**, *62*, 202214383.
[152] C. A. Giron Rodriguez, B. Ó. Joensen, A. B. Moss, G. O. Larrazábal, D. K. Whelligan, B. Seger, J. R. Varcoe, T. R. Willson, *ACS Sustainable Chem. Eng.* **2023**, *11*, 1508.

[153] Q. Lu, J. Rosen, Y. Zhou, G. S. Hutchings, Y. C. Kimmel, J. G. Chen, F. Jiao, *Nat. Commun.* **2014**, *5*, 3242.
[154] S. Jovanovic, R. Krause, A. Lüken, J. Ackermann, S. Merz, P. Jakes, R.-A. Eichel, J. Granwehr, *J. Electrochem. Soc.* **2020**, *167*, 086505.
[155] B. Nourmohammadi Khiarak, G. T. S. T. Da Silva, V. Grange, G. Gao, V. Golovanova, F. P. de García Arquer, L. H. Mascaro, C.-T. Dinh, *Small* **2025**, *21*, 2409669.
[156] Y. Mao, S. Chen, Z. Jia, X. Dong, Q. Mao, *Chem. Res. Chin. Univ.* **2023**, *39*, 1031.
[157] X. Peng, S. G. Karakalos, W. E. Mustain, *ACS Appl. Mater. Interfaces* **2018**, *10*, 1734.
[158] M. C. Paulisch, M. Gebhard, D. Franzen, A. Hilger, M. Osenberg, S. Marathe, C. Rau, B. Ellendorff, T. Turek, C. Roth, I. Manke, *ACS Appl. Energy Mater.* **2021**, *4*, 7497.
[159] S. Li, X. Dong, G. Wu, Y. Song, J. Mao, A. Chen, C. Zhu, G. Li, Y. Wei, X. Liu, J. Wang, W. Chen, W. Wei, *Nat. Commun.* **2024**, *15*, 6101.
[160] E. Gräfin von Westarp, B. Hecker, H. Tempel, R.-A. Eichel, *Electrochem. Sci. Adv.* **2024**, 202400017.
[161] O. Romiluyi, N. Danilovic, A. T. Bell, A. Z. Weber, *Electrochem. Sci. Adv.* **2023**, *3*, 2100186.
[162] A. A. Samu, I. Szenti, Á. Kukovecz, B. Endrődi, C. Janáky, *Commun. Chem.* **2023**, *6*, 41.
[163] M. Yang, J. Zhang, Y. Cao, M. Wu, K. Qian, Z. Zhang, H. Liu, J. Wang, W. Chen, W. Huang, *ChemCatChem* **2018**, *10*, 5128.
[164] F. Lai, X. Wang, Z. Liu, C. Wang, H. Sun, B. Geng, *ACS Sustainable Chem. Eng.* **2021**, *9*, 6756.
[165] E. R. Cofell, Z. Park, U. O. Nwabara, L. C. Harris, S. S. Bhargava, A. A. Gewirth, P. J. A. Kenis, *ACS Appl. Energy Mater.* **2022**, *5*, 12013.
[166] C. Cai, B. Liu, K. Liu, P. Li, J. Fu, Y. Wang, W. Li, C. Tian, Y. Kang, A. Stefancu, H. Li, C.-W. Kao, T.-S. Chan, Z. Lin, L. Chai, E. Cortés, M. Liu, *Angew. Chem., Int. Ed.* **2022**, *61*, 202212640.
[167] J. Gao, C. Zhu, M. Zhu, Y. Fu, H. Huang, Y. Liu, Z. Kang, *ACS Sustainable Chem. Eng.* **2019**, *7*, 3536.
[168] M. Duarte, B. de Mot, J. Hereijgers, T. Breugelmans, *ChemElectroChem* **2019**, *6*, 5596.
[169] D. McLaughlin, M. Bierling, B. Mayerhöfer, G. Schmid, S. Thiele, *Adv. Funct. Mater.* **2023**, *33*, 2212462.
[170] L. M. Baumgartner, A. Kahn, M. Hoogland, J. Bleeker, W. F. Jager, D. A. Vermaas, *ACS Sustainable Chem. Eng.* **2023**, *11*, 10430.
[171] J. Lee, W. Lee, K. H. Ryu, J. Park, H. Lee, J. H. Lee, K. T. Park, *Green Chem.* **2021**, *23*, 2397.
[172] Y. Xue, Y. Zhu, C. He, K. Wu, Y. Liu, B. Wang, H. Lu, B. Liang, *Chem. Commun.* **2024**, *60*, 4934.
[173] C.-Y. Lee, J. Zou, G. G. Wallace, *Mater. Today Chem.* **2024**, *38*, 102117.
[174] S. Li, Z. Xiao, Y. Shi, L. Zhang, J. Li, Q. Fu, X. Zhu, Q. Liao, *Energy Convers. Manage.* **2024**, *321*, 119029.
[175] Z. Zhang, Y. Luo, X. Hu, Z. Li, Y. Wu, W. Wei, Y. Wang, X.-K. Gu, J. Xu, M. Ding, *J. Colloid Interface Sci.* **2025**, *683*, 468.
[176] Q. Chang, G. Zhang, Y. Wang, Y. Lin, H. Gao, L. Guo, P. Zhang, C. Pei, T. Wang, J. Gong, *Adv. Funct. Mater.* **2025**, *35*, 2425601.
[177] Y. Xu, J. P. Edwards, S. Liu, R. K. Miao, J. E. Huang, C. M. Gabardo, C. P. O'Brien, J. Li, E. H. Sargent, D. Sinton, *ACS Energy Lett.* **2021**, *6*, 809.
[178] S. Garg, M. Li, T. Hussain, M. N. Idros, Y. Wu, X. S. Zhao, G. G. X. Wang, T. E. Rufford, *ACS Appl. Mater. Interfaces* **2022**, *14*, 35504.
[179] M. A. A. Mahbub, D. Das, X. Wang, G. Lu, M. Muhler, W. Schuhmann, *Angew. Chem., Int. Ed.* **2025**, *64*, 202419775.
[180] Y. Qin, W. Qian, J. Zhang, X. Chen, M. Chen, X. Qin, C. Zhang, *Electrochim. Acta* **2025**, *514*, 145637.
[181] J. Lee, J. Lim, C.-W. Roh, H. S. Whang, H. Lee, *J. CO2 Util.* **2019**, *31*, 244.
[182] C. M. Gabardo, A. Seifitokaldani, J. P. Edwards, C.-T. Dinh, T. Burdyny, M. G. Kibria, C. P. O'Brien, E. H. Sargent, D. Sinton, *Energy Environ. Sci.* **2018**, *11*, 2531.
[183] K. Jiang, P. Kharel, Y. Peng, M. K. Gangishetty, H.-Y. G. Lin, E. Stavitski, K. Attenkofer, H. Wang, *ACS Sustainable Chem. Eng.* **2017**, *5*, 8529.
[184] B. Ameduri, *Perfluoroalkyl substances. Synthesis, applications, challenges and regulations*, Royal Society of Chemistry, Cambridge, UK, **2022**.
[185] S. F. Hansen, C. T. H. Bunde, M. A. Roy, J. A. Tickner, A. Baun, *Nat. Water* **2024**, *2*, 1157.
[186] C. Yu, T. Lei, Li Xu, C. Jin, J. Yi, S. Liu, S. Lin, Y. Yang, H. Song, K. Wang, H. Fan, C. Zheng, X. Zhang, X. Gao, *J. Mater. Chem. A* **2024**, *12*, 17181.
[187] P. von Tettau, P. Thiele, P. Mauermann, M. Wick, S. Tinz, S. Pischinger, *J. Power Sources* **2025**, *630*, 236104.
[188] Y. S. Ham, Y. S. Park, A. Jo, J. H. Jang, S.-K. Kim, J. J. Kim, *J. Power Sources* **2019**, *437*, 226898.
[189] A. Jo, S. Kim, H. Park, H.-Y. Park, J. Hyun Jang, H. S. Park, *J. Catal.* **2021**, *393*, 92.
[190] A. Alihosseinzadeh, A. Unnikrishnan, K. Karan, S. Ponnurangam, *ACS Appl. Energy Mater.* **2023**, *6*, 1533.
[191] C. Tang, P. Gong, T. Xiao, Z. Sun, *Nat. Commun.* **2021**, *12*, 2139.
[192] Z. Xie, Y. Qiu, S. Gao, J. Sun, H. Cao, S. Zhang, J. Luo, X. Liu, *ChemElectroChem* **2021**, *8*, 3579.
[193] J. Sun, B. Yu, X. Yan, J. Wang, F. Tan, W. Yang, G. Cheng, Z. Zhang, *Materials* **2022**, *15*, 6892.
[194] C. Larrea, J. R. Avilés-Moreno, P. Ocón, *Molecules* **2023**, *28*, 1951.
[195] D Un Lee, B. Joensen, J. Jenny, V M. Ehlinger, S.-W. Lee, K. Abiose, Yi Xu, A. Sarkar, T Y. Lin, C. Hahn, T F. Jaramillo, *ACS Sustainable Chem. Eng.* **2023**, *11*, 16661.
[196] K. Wu, E. Birgersson, B. Kim, P. J. A. Kenis, I. A. Karimi, *J. Electrochem. Soc.* **2015**, *162*, F23.
[197] N. T. Nesbitt, W. A. Smith, *J. Electrochem. Soc.* **2021**, *168*, 044505.
[198] X. Jiang, H. Wu, S. Chang, R. Si, S. Miao, W. Huang, Y. Li, G. Wang, X. Bao, *J. Mater. Chem. A* **2017**, *5*, 19371.
[199] Z. Wang, T. Li, Q. Wang, A. Guan, N. Cao, A. M. Al-Enizi, L. Zhang, L. Qian, G. Zheng, *J. Power Sources* **2020**, *476*, 228705.
[200] H. W. Shafaque, C. Lee, K. F. Fahy, J. K. Lee, J. M. LaManna, E. Baltic, D. S. Hussey, D. L. Jacobson, A. Bazylak, *ACS Appl. Mater. Interfaces* **2020**, *12*, 54585.
[201] X. Yuan, Y. Wu, B. Jiang, Z. Wu, Z. Tao, X. Lu, J. Liu, T. Qian, H. Lin, Q. Zhang, *ACS Appl. Mater. Interfaces* **2020**, *12*, 56642.
[202] Y. Chen, F. Hu, Y. Hao, Y. Wang, Y. Xie, H. Wang, L. Yin, D. Yu, H. Yang, J. Ma, D. Kai, L. Li, S. Peng, *Nano Res.* **2022**, *15*, 3283.
[203] D. Krisch, H. Sun, K. Pellumbi, K. Faust, U.-P. Apfel, W. Schöfberger, *Catalysts* **2022**, *12*, 545.
[204] Y. Kong, M. Liu, H. Hu, Y. Hou, S. Vesztergom, M. d. J. Gálvez-Vázquez, I. Zelocualtecatl Montiel, V. Kolivoška, P. Broekmann, *Small Methods* **2022**, *6*, 2200369.
[205] Y C. Li, G. Lee, T. Yuan, Y. Wang, D.-H. Nam, Z. Wang, F. P García de Arquer, Y. Lum, C.-T. Dinh, O. Voznyy, E H. Sargent, *ACS Energy Lett.* **2019**, *4*, 1427.
[206] K. Seteiz, J. N. Häberlein, P. A. Heizmann, L. Bohn, S. Vierrath, J. Disch, *ACS Appl. Eng. Mater.* **2024**, *2*, 1654.
[207] T. Bi, R. Xue, Y. Jiang, S. Yuan, C. Zhao, G. Zhang, X. Cheng, J. Yin, G. Wei, X. Yan, J. Zhang, *Int. J. Hydrogen Energy* **2024**, *90*, 784.
[208] J. W. Sun, T. Yu, H. Wu, M. Zhu, A. Chen, C. Lian, H. G. Yang, P. F. Liu, *Chem Catal* **2024**, *4*, 100923.
[209] Y. Wu, M. N. Idros, D. Feng, W. Huang, T. Burdyny, B. Wang, G. Wang, M. Li, T. E. Rufford, *ACS Appl. Mater. Interfaces* **2024**, *16*, 56967.
[210] X. Wu, Y. Guo, Z. Sun, F. Xie, D. Guan, J. Dai, F. Yu, Z. Hu, Yu-C Huang, C.-W. Pao, J.-L. Chen, W. Zhou, Z. Shao, *Nat. Commun.* **2021**, *12*, 660.
[211] Z. Cai, Y. Wu, Z. Wu, L. Yin, Z. Weng, Y. Zhong, W. Xu, X. Sun, H. Wang, *ACS Energy Lett.* **2018**, *3*, 2816.

[212] A. Ozden, Y. Liu, C.-T. Dinh, J. Li, P. Ou, F. P. García de Arquer, E. H. Sargent, D. Sinton, *ACS Appl. Energy Mater.* **2021**, *4*, 7504.
[213] C. P. O'Brien, R. K. Miao, S. Liu, Y. Xu, G. Lee, A. Robb, J. E. Huang, K. Xie, K. Bertens, C. M. Gabardo, J. P. Edwards, C. T. Dinh, E. H. Sargent, D. Sinton, *ACS Energy Lett.* **2021**, *6*, 2952.
[214] X. Zhu, J. Jack, Y. Bian, X. Chen, N. Tsesmetzis, Z. J. Ren, *ACS Sustainable Chem. Eng.* **2021**, *9*, 6012.
[215] A. Senocrate, F. Bernasconi, D. Rentsch, K. Kraft, M. Trottmann, A. Wichser, D. Bleiner, C. Battaglia, *ACS Appl. Energy Mater.* **2022**, *5*, 14504.
[216] Y. Pu, Y. Wang, G. Wu, X. Wu, Y. Lu, Y. Yu, Na Chu, X. He, D. Li, R. J. Zeng, Y. Jiang, *Environ. Sci. Technol.* **2024**, *58*, 7445.
[217] B. Pan, J. Fan, J. Zhang, Y. Luo, C. Shen, C. Wang, Y. Wang, Y. Li, *ACS Energy Lett.* **2022**, *7*, 4224.
[218] J.-Z. Zhang, S. Wu, F. Shen, W. Song, Y. Hua, Z. Wu, X.-G. Zhang, J. Shi, *Ionics* **2022**, *28*, 4321.
[219] H. Hoffmann, M. Kutter, J. Osiewacz, M.-C. Paulisch-Rinke, S. Lechner, B. Ellendorff, A. Hilgert, I. Manke, T. Turek, C. Roth, *EES Catal.* **2024**, *2*, 286.
[220] J. P. Edwards, Y. Xu, C. M. Gabardo, C.-T. Dinh, J. Li, Z. Qi, A. Ozden, E. H. Sargent, D. Sinton, *Appl. Energy* **2020**, *261*, 114305.
[221] W. Lai, Y. Qiao, Y. Wang, H. Huang, *Adv. Mater.* **2023**, *35*, 2306288.
[222] A. J. Martín, G. O. Larrazábala, J. Pérez-Ramírez, *Green Chem.* **2015**, *2015*, 5114.
[223] Z. Zhang, Q. Lu, J. Sun, G. Li, W. Wu, Z. Xu, L. Xu, Y. Wang, *Chem. Sci.* **2024**, *15*, 2786.
[224] Y. Sun, J. Chen, X. Du, J. Cui, X. Chen, C. Wu, X. Yang, L. Liu, J. Ye, *Angew. Chem., Int. Ed.* **2024**, *63*, 202410802.
[225] S. Verma, B. Kim, H.-R. M. Jhong, S. Ma, P. J. A. Kenis, *ChemSusChem* **2016**, *9*, 1972.
[226] M. Jouny, W. Luc, F. Jiao, *Ind. Eng. Chem. Res.* **2018**, *57*, 2165.
[227] G. Wen, B. Ren, X. Wang, D. Luo, H. Dou, Y. Zheng, R. Gao, J. Gostick, A. Yu, Z. Chen, *Nat. Energy* **2022**, *7*, 978.
[228] Z. Li, X. Li, R. Wang, A. Campos Mata, C S. Gerke, S. Xiang, A. Mathur, L. Zhang, D.-Z. Lin, T. Li, K N. Jayarapu, A. Liu, L. Gupta, A I. Frenkel, V. S Thoi, P M. Ajayan, S. Roy, Y. Liu, Y. Liu, *Nat. Commun.* **2025**, *16*, 3206.
[229] B. Hasa, Y. Zhao, F. Jiao, *Annu. Rev. Chem. Biomol. Eng.* **2023**, *14*, 165.
[230] S. Vijay, W. Ju, S. Brückner, S.-C. Tsang, P. Strasser, K. Chan, *Nat. Catal.* **2021**, *4*, 1024.
[231] E. L. Clark, S. Ringe, M. Tang, A. Walton, C. Hahn, T. F. Jaramillo, K. Chan, A. T. Bell, *ACS Catal.* **2019**, *9*, 4006.
[232] T. Zhang, X. Lu, W. Qi, G. Qin, S. Li, *Appl. Catal. B* **2024**, *349*, 123896.
[233] M. Abdinejad, E. Irtem, A. Farzi, M. Sassenburg, S. Subramanian, H.-P. Iglesias van Montfort, D. Ripepi, M. Li, J. Middelkoop, A. Seifitokaldani, T. Burdyny, *ACS Catal.* **2022**, *12*, 7862.
[234] Y.-J. Ko, C. Lim, J. Jin, M. G. Kim, Ji Y Lee, T.-Y. Seong, K.-Y. Lee, B. K. Min, J.-Y. Choi, T. Noh, G. W. Hwang, W. H. Lee, H.-S. Oh, *Nat. Commun.* **2024**, *15*, 3356.
[235] E. Boutin, S. Haussener, *ACS Catal.* **2024**, *14*, 8437.
[236] H. Huang, R. Shi, Z. Li, J. Zhao, C. Su, T. Zhang, *Angew. Chem., Int. Ed.* **2022**, *61*, 202200802.
[237] H. Huang, Q. Zhang, R. Shi, C. Su, Y. Wang, J. Zhao, T. Zhang, *Appl. Catal. B* **2022**, *317*, 121731.
[238] A. J. Welch, A. Q. Fenwick, A. Böhme, H.-Y. Chen, I. Sullivan, X. Li, J. S. DuChene, C. Xiang, H. A. Atwater, *J. Phys. Chem. C* **2021**, *125*, 20896.
[239] J. den Hollander, W. van der Stam, *Curr. Opin. Chem. Eng.* **2023**, *42*, 100979.
[240] F. Bienen, D. Kopljar, A. Löwe, S. Geiger, N. Wagner, E. Klemm, K. A. Friedrich, *ACS Sustainable Chem. Eng.* **2020**, *8*, 13759.
[241] N. J. Firet, T. Burdyny, N. T. Nesbitt, S. Chandrashekar, A. Longo, W. A. Smith, *Catal. Sci. Technol.* **2020**, *10*, 5870.
[242] X. Lu, C. Zhu, Z. Wu, J. Xuan, J. S. Francisco, H. Wang, *J. Am. Chem. Soc.* **2020**, *142*, 15438.
[243] S. Jovanovic, P. Jakes, S. Merz, D. T. Daniel, R.-A. Eichel, J. Granwehr, *Commun. Chem.* **2023**, *6*, 268.
[244] J. J. Kaczur, H. Yang, Z. Liu, S. D. Sajjad, R. I. Masel, *Front. Chem.* **2018**, *6*, 263.
[245] R. Küngas, *J. Electrochem. Soc.* **2020**, *167*, 44508.
[246] Q. Chen, A. Kube, D. Kopljar, K. A. Friedrich, *ACS Energy Lett.* **2024**, *9*, 6096.
[247] M. Pfennig, B. Schiffer, T. Clees, *Int. J. Hydrogen Energy* **2025**, *104*, 567.
[248] Siemens A. G., "CO2 for a clean performance: Rheticus research project enters phase 2", (accessed: April **2025**).
[249] M. Quentmeier, B. Schmid, H. Tempel, R.-A. Eichel, *ACS Sustainable Chem. Eng.* **2024**, *12*, 3876.
[250] V. E. Nelson, C. P. O'Brien, J. P. Edwards, S. Liu, C. M. Gabardo, E. H. Sargent, D. Sinton, *ACS Appl. Mater. Interfaces* **2024**, *16*, 50818.
[251] J P. Edwards, T. Alerte, C P. O'Brien, C M. Gabardo, S. Liu, J. Wicks, A. Gaona, J. Abed, Y. C. Xiao, D. Young, A. Sedighian Rasouli, A. Sarkar, S A. Jaffer, H L. MacLean, E H. Sargent, D. Sinton, *ACS Energy Lett.* **2023**, *8*, 2576.
[252] S. Oh, H. Park, H. Kim, Y. S. Park, M. G. Ha, J. H. Jang, S.-K. Kim, *Coatings* **2020**, *10*, 341.
[253] P. Wilde, A. Özden, H. Winter, T. Quast, J. Weidner, S. Dieckhöfer, J. R. C. Junqueira, M. Metzner, W. Peter, W. Leske, D. Öhl, T. Bobrowski, T. Turek, W. Schuhmann, *Appl. Res.* **2023**, *2*, 202200081.
[254] M. Filippi, T. Möller, R. Pastusiak, E. Magori, B. Paul, P. Strasser, *ACS Energy Lett.* **2024**, *9*, 1361.
[255] H.-R. Jhong, F. R. Brushett, P. J. A. Kenis, *Adv. Energy Mater.* **2013**, *3*, 589.
[256] W. Guo, K. Shim, Y.-T. Kim, *Appl. Surf. Sci.* **2020**, *526*, 146651.
[257] C. Corbella, A. Aijaz, T. Kubart, L. Lin, S. Portal, M. Keidar, *Carbon* **2025**, *232*, 119772.
[258] E. Jeng, Z. Qi, A R. Kashi, S. Hunegnaw, Z. Huo, J S. Miller, L B. Bayu Aji, B. H. Ko, H. Shin, S. Ma, K P. Kuhl, F. Jiao, J. Biener, *ACS Appl. Mater. Interfaces* **2022**, *14*, 7731.
[259] B. Lee, J. G. Kim, C. Pak, *Korean J. Chem. Eng.* **2020**, *37*, 2334.
[260] Y. Devi, P.-J. Huang, W.-T. Chen, R.-H. Jhang, C.-H. Chen, *ACS Appl. Mater. Interfaces* **2023**, *15*, 9231.
[261] S A. Mauger, M. Wang, F C. Cetinbas, M J. Dzara, J. Park, D J. Myers, R K. Ahluwalia, S. Pylypenko, L. Hu, S. Litster, K. C. Neyerlin, M. Ulsh, *J. Power Sources* **2021**, *506*, 230039.
[262] T. Turek, I. Moussallem, A. Bulan, N. Schmitz, P. Weuta, US9243337B2, Covestro Deutschland AG, Leverkusen, Germany, **2016**.
[263] S. Rufer, M. P. Nitzsche, S. Garimella, J. R. Lake, K. K. Varanasi, *Nat. Commun.* **2024**, *15*, 9429.
[264] H.-P. Iglesias van Montfort, M. Li, E. Irtem, M. Abdinejad, Y. Wu, S K. Pal, M. Sassenburg, D. Ripepi, S. Subramanian, J. Biemolt, T E. Rufford, T. Burdyny, *Nat. Commun.* **2023**, *14*, 6579.
[265] A. Ross, M. Muñoz, B. H. Rotstein, E. J. Suuronen, E. I. Alarcon, *Sci. Rep.* **2021**, *11*, 5420.
[266] D. Segets, C. Andronescu, U.-P. Apfel, *Nat. Commun.* **2023**, *14*, 7950.
[267] M. R. Singh, J. D. Goodpaster, A. Z. Weber, M. Head-Gordon, A. T. Bell, *Proc. Natl. Acad. Sci. U.S.A.* **2017**, *114*, E8812.
[268] T. Nann, J. Heinze, *Electrochem. Commun.* **1999**, *1*, 289.
[269] G. Bauer, V. Gravemeier, W. A. Wall, *Int. J. Numer. Methods Eng.* **2011**, *86*, 1339.
[270] A. N. Colli, J. M. Bisang, *J. Electrochem. Soc.* **2022**, *169*, 034524.
[271] L.-C. Weng, A. T. Bell, A. Z. Weber, *Phys. Chem. Chem. Phys.* **2018**, *20*, 16973.

[272] J. W. Blake, J. T. Padding, J. W. Haverkort, *Electrochim. Acta* **2021**, *393*, 138987.
[273] E. W. Lees, J. C. Bui, O. Romiluyi, A. T. Bell, A. Z. Weber, *Nat. Chem. Eng.* **2024**, *1*, 340.
[274] M. Löffelholz, J. Osiewacz, A. Lüken, K. Perrey, A. Bulan, T. Turek, *Chem. Eng. J.* **2022**, *435*, 134920.
[275] R. Kas, A. G. Star, K. Yang, T. van Cleve, K. C. Neyerlin, W. A. Smith, *ACS Sustainable Chem. Eng.* **2021**, *9*, 1286.
[276] V. Kannan, K. A. Raman, A. Fisher, E. Birgersson, *Ind. Eng. Chem. Res.* **2019**, *58*, 19361.
[277] L.-C. Weng, A. T. Bell, A. Z. Weber, *Energy Environ. Sci.* **2019**, *12*, 1950.
[278] J. C. Bui, E. W. Lees, L. M. Pant, I. V. Zenyuk, A. T. Bell, A. Z. Weber, *Chem. Rev.* **2022**, *122*, 11022.
[279] Y. Du, Y. Qin, G. Zhang, Y. Yin, K. Jiao, Q. Du, *Int. J. Hydrogen Energy* **2019**, *44*, 3456.
[280] X. Y. Tai, L. Xing, Y. Zhang, Q. Fu, O. Fisher, S. D. Christie, J. Xuan, *Digit. Chem. Eng.* **2023**, *9*, 100123.
[281] K. A. Raman, L. Hammacher, H. Kungl, A. Karl, E. Jodat, R.-A. Eichel, V. Karyofylli, *Appl. Energy* **2025**, *386*, 125529.
[282] G. James, D. Witten, T. Hastie, R. Tibshirani, *An introduction to Statistical Learning*, Springer, New York **2013**.
[283] T. Sutharssan, D. Montalvao, Y. K. Chen, W.-C. Wang, C. Pisac, H. Elemara, *Renew. Sustain. Energy Rev.* **2017**, *75*, 440.
[284] I. Grega, F. Therrien, A. Soni, K. Ocean, K. Dettelbach, R. Ahmadi, M. Mokhtari, C. P. Berlinguette, Y. Bengio, arXiv preprint **2025**, arXiv:2502.06323.
[285] L. Xing, H. Jiang, X. Tian, H. Yin, W. Shi, E. Yu, V. J. Pinfield, J. Xuan, *Carbon Capture Sci. Technol.* **2023**, *9*, 100138.
[286] A. B. Owen, *SIAM/ASA J. U. Quantif.* **2014**, *2*, 245.
[287] G. Zhang, X. Liu, H. Lei, Y. Wang, D. Bildan, X. Zhuge, L. Xing, K. Luo, *Fuel* **2024**, *373*, 132400.
[288] C. Song, R. Kawai, *Probab. Eng. Mech.* **2023**, *73*, 103479.
[289] D. Dogan, B. Hecker, X. Hou, I. Dessel, A. Müller, G. Wasserschaff, S S. Köcher, V. Karyofylli, H. Kungl, H. Tempel, R-A. Eichel, *Electrochem. Sci. Adv.* **2024**, 202400015.
[290] J. W. Blake, V. Konderla, L. M. Baumgartner, D. A. Vermaas, J. T. Padding, J. W. Haverkort, *ACS Sustainable Chem. Eng.* **2023**, *11*, 2840.
[291] M. Bahreini, M. Désilets, E. Pahija, U. Legrand, *Chem. Eng. J. Adv.* **2025**, *23*, 100816.
[292] R. Ding, S. Zhang, Y. Chen, Z. Rui, K. Hua, Y. Wu, X. Li, X. Duan, X. Wang, J. Li, J. Liu, *Energy AI* **2022**, *9*, 100170.
[293] K. A. Raman, N. L. Wolf, A. Javed, V. Karyofylli, H. Kungl, A. Karl, E. Jodat, R.-A. Eichel, *Energy A. I.* **2025**, *22*, 100623.
[294] S. Zhou, R. Jervis, *Chem. Methods* **2024**, *4*, 202300030.
[295] A. Javed, N. L. Wolf, F. Meyer, L. Treutlein, H. Kungl, A. Karl, E. Jodat, R.-A. Eichel, *Int. J. Hydrogen Energy* **2025**, *98*, 280.
[296] Y. He, S. Liu, M. Wang, H. Ji, L. Zhang, Q. Cheng, T. Qian, C. Yan, *Adv. Funct. Mater.* **2022**, *32*, 2208474.
[297] Y. He, M. Wang, H. Ji, Q. Cheng, S. Liu, Y. Huan, T. Qian, C. Yan, *Adv. Funct. Mater.* **2025**, *35*, 2413703.
[298] A. Weiß, A. Siebel, M. Bernt, T.-H. Shen, V. Tileli, H. A. Gasteiger, *J. Electrochem. Soc.* **2019**, *166*, F487.
[299] A. A. Samu, A. Kormányos, E. Kecsenovity, N. Szilágyi, B. Endrődi, C. Janáky, *ACS Energy Lett.* **2022**, *7*, 1859.